RESEARCH ARTICLE

Targeting the p300/CBP Axis in Lethal Prostate Cancer

Jonathan Welti[1], Adam Sharp[1,2], Nigel Brooks[3], Wei Yuan[1], Christopher McNair[4], Saswati N. Chand[4], Abhijit Pal[2], Ines Figueiredo[1], Ruth Riisnaes[1], Bora Gurel[1], Jan Rekowski[1], Denisa Bogdan[1], William West[3], Barbara Young[5], Meera Raja[5], Amy Prosser[5], Jordan Lane[5], Stuart Thomson[5], Jenny Worthington[6], Stuart Onions[5], Jonathan Shannon[5], Silvia Paoletta[5], Richard Brown[5], Don Smyth[5], Gareth W. Harbottle[5], Veronica S. Gil[1], Susana Miranda[1], Mateus Crespo[1], Ana Ferreira[1], Rita Pereira[1], Nina Tunariu[2], Suzanne Carreira[1], Antje J. Neeb[1], Jian Ning[1], Amanda Swain[1], David Taddei[5], SU2C/PCF International Prostate Cancer Dream Team, Matthew J. Schiewer[4], Karen E. Knudsen[4], Neil Pegg[3], and Johann S. de Bono[1,2]

ABSTRACT

Resistance to androgen receptor (AR) blockade in castration-resistant prostate cancer (CRPC) is associated with sustained AR signaling, including through alternative splicing of AR (AR-SV). Inhibitors of transcriptional coactivators that regulate AR activity, including the paralog histone acetyltransferase proteins p300 and CBP, are attractive therapeutic targets for lethal prostate cancer. Herein, we validate targeting p300/CBP as a therapeutic strategy for lethal prostate cancer and describe CCS1477, a novel small-molecule inhibitor of the p300/CBP conserved bromodomain. We show that CCS1477 inhibits cell proliferation in prostate cancer cell lines and decreases AR- and C-MYC–regulated gene expression. In AR-SV–driven models, CCS1477 has antitumor activity, regulating AR and C-MYC signaling. Early clinical studies suggest that CCS1477 modulates KLK3 blood levels and regulates CRPC biopsy biomarker expression. Overall, CCS1477 shows promise for the treatment of patients with advanced prostate cancer.

SIGNIFICANCE: Treating CRPC remains challenging due to persistent AR signaling. Inhibiting transcriptional AR coactivators is an attractive therapeutic strategy. CCS1477, an inhibitor of p300/CBP, inhibits growth and AR activity in CRPC models, and can affect metastatic CRPC target expression in serial clinical biopsies.

See related commentary by Rasool et al., p. 1011.

[1]The Institute of Cancer Research, London, United Kingdom. [2]The Royal Marsden Hospital, London, United Kingdom. [3]CellCentric Ltd., Cambridge, United Kingdom. [4]Thomas Jefferson University, Philadelphia, Pennsylvania. [5]Sygnature Discovery Services, Nottingham, United Kingdom. [6]Axis Bioservices, Coleraine, Northern Ireland.

Note: Supplementary data for this article are available at Cancer Discovery Online (http://cancerdiscovery.aacrjournals.org/).

J. Welti, A. Sharp, and N. Brooks contributed equally to this article.

N. Pegg and J.S. de Bono are the co-senior authors of this article.

Corresponding Author: Johann de Bono, The Institute of Cancer Research, 15 Cotswold Road, London SM2 5NG, United Kingdom. Phone: 4402-0872-24029; Fax: 4402-0864-27979; E-mail: johann.de-bono@icr.ac.uk

Cancer Discov 2021;11:1118–37

doi: 10.1158/2159-8290.CD-20-0751

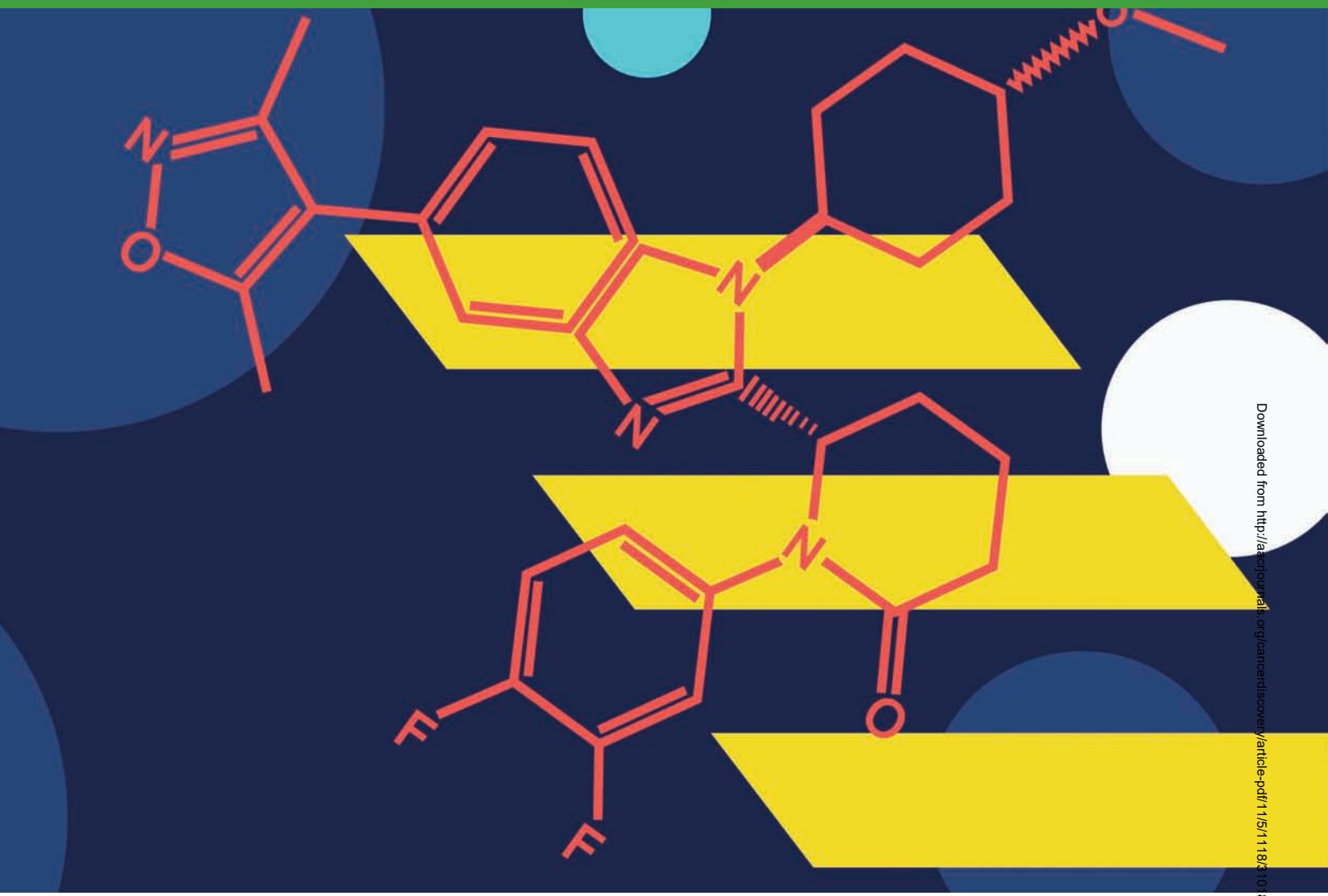

INTRODUCTION

Prostate cancer, one of the most common malignancies in men, is a leading cause of male cancer-related death globally and is rapidly increasing in incidence in Asia (1). Prostate carcinogenesis, as well as prostate tumor growth, is driven by activation of the androgen receptor (AR; refs. 2–4). The AR, a nuclear steroid hormone receptor, functions as a transcription factor that regulates the expression of multiple genes that are key to prostate cancer growth and proliferation. Consistent with this, therapies that target AR signaling have been successful in improving the outcome of patients with castration-sensitive and castration-resistant prostate cancer (CRPC; refs. 5–8). Despite this, advanced prostate cancer remains fatal and improved therapeutic strategies remain an urgent unmet medical need.

The development and progression of CRPC is characterized by continued AR signaling through either overexpression of the AR, mutations of the AR ligand-binding domain, tumor-derived androgen production, expression of constitutively active AR splice variants (AR-SV) of which AR-V7 remains the best studied, or increased expression of AR coregulators including the transcription factor coactivator proteins p300/CBP (9–26). p300 and CBP are paralogous, highly conserved proteins that serve as transcriptional regulators. Their functional activity is, at least in part, mediated by two conserved regions: a catalytic histone acetyltransferase domain and a bromodomain. These domains interact with a plethora of transcription factors, as well as the general transcriptional machinery, and therefore regulate multiple cellular processes (27). Importantly, they have been described as potent coactivators of the AR, and perturbation of p300/CBP function in prostate cancer models has been reported to decrease AR function and reduce tumor cell growth (25, 28–38). Taken together, targeting p300/CBP is an attractive therapeutic strategy to abrogate persistent AR signaling in advanced prostate cancer.

Herein, we show for the first time that targeting p300/CBP blocks AR and AR-SV signaling, and we characterize an orally bioavailable, potent, and selective inhibitor of the p300/CBP bromodomain CCS1477. We demonstrate that CCS1477 affects AR and MYC signaling in cell line and patient-derived xenografts, as well as in serial tumor biopsies acquired from an ongoing first-in-human phase I trial (NCT03568656).

RESULTS

CBP and p300 mRNA in Primary and Castration-Resistant Prostate Cancer

Because CBP and p300 are known coactivators of the AR, which enhance AR activity, we determined the association of CBP and p300 mRNA expression with an AR signature in primary prostate cancer and metastatic castration-resistant prostate cancer (mCRPC; refs. 30, 33, 34, 38). The AR signature was determined using two previously described gene-expression signatures (Supplementary Table S1; refs. 39, 40). Analysis of mRNA sequencing data from 550 primary prostate cancer samples and 120 mCRPC samples demonstrated that CBP and p300 mRNA expression significantly (all $P \leq 0.001$) associated with the AR signature in primary prostate cancer and mCRPC (Fig. 1A–D; refs. 41, 42). In addition, CBP and p300 mRNA expression significantly (all $P \leq 0.001$) associated with AR mRNA expression (Supplementary Fig. S1A–S1D). Consistent with these data, and their role in AR activation, CBP and p300 mRNA expression significantly (all $P \leq 0.001$) associated with a previously described acquired androgen deprivation therapy (ADT) resistance signature in primary prostate cancer and mCRPC (Fig. 1E–H; Supplementary Table S2; ref. 43). Furthermore, we also identified CBP and p300 mRNA expression, along with AR mRNA expression, to be highly expressed in primary prostate cancer and mCRPC biopsies (Fig. 1I; Supplementary Fig. S1E; refs. 25, 26, 41), with CBP and p300 mRNA expression being significantly ($P \leq 0.001$) coexpressed in mCRPC (Supplementary Fig. S1F). Taken together, these results support the interrogation of targeting p300 and CBP as a means to block AR signaling in prostate cancer.

CBP and p300 Protein in Castration-Sensitive and Castration-Resistant Prostate Cancer

To investigate nuclear CBP and p300 protein expression in prostate cancer, we evaluated tumor samples from 43 patients with matched castration-sensitive prostate cancer (CSPC) and CRPC biopsies (Supplementary Table S3). CBP and p300 antibody specificity for IHC was confirmed using siRNA knockdown in HeLa cells (Supplementary Fig. S2A and S2B). H-scores (HS) were determined by IHC for nuclear CBP and p300 protein expression in all patient biopsies (Fig. 1J–L). Nuclear CBP protein expression did not significantly ($P = 0.28$) change as tumors progressed from CSPC [median; interquartile range (IQR): HS 100; 50–160] to CRPC (HS 140; 80–180; Fig. 1J and K). Similarly, nuclear p300 protein expression did not significantly ($P = 0.09$) change as tumors progressed from CSPC (median; IQR: HS 110; 75–170) to CRPC (HS 115; 80–175; Fig. 1J and L). However, all 43 patients had tumors expressing nuclear CBP and p300 protein at CRPC, and, consistent with the mRNA expression data, there was a significant ($r = 0.50$; 95% CI, 0.22–0.70; $P \leq 0.001$) association between nuclear CBP and p300 protein expression (Supplementary Fig. S2C). Following this, HS were determined by IHC for nuclear full-length AR (AR-FL; 41 patients) and AR-V7 (43 patients) protein expression in CRPC using already-validated assays (44). Nuclear CBP and p300 protein expression did not significantly correlate with nuclear AR-FL or AR-V7 protein expression in CRPC (Supplementary Fig. S2D–S2G). Interestingly, in patients who did not receive treatment with curative intent (radiotherapy or surgery) at diagnosis ($n = 27$), patients with lower nuclear p300 protein expression (HS $\leq$ 123.3; $n = 18$) at CSPC had a significantly longer median time to CRPC [21.0 vs. 10.1 months; hazard ratio (HR), 0.25; 95% CI, 0.08–0.83; $P \leq 0.001$], and a trend toward improved overall survival (50.9 vs. 37.2 months; HR, 0.51; 95% CI, 0.18–1.48; $P = 0.12$), when compared to those patients with higher nuclear p300 protein expression (HS > 123.3; $n = 9$; Supplementary Fig. S2H–S2I). In contrast, nuclear CBP protein expression at diagnosis had no impact on time to CRPC or overall survival in those patients treated with systemic therapy alone (Supplementary Fig. S2J and S2K). These data suggest that CBP and p300 are highly expressed, and that p300 may affect benefit from prostate cancer endocrine treatments.

CBP and p300 Knockdown Regulates AR Signaling in a C-MYC–Independent Manner in Cell Line Models of CRPC

Having shown that CBP and p300 are highly expressed and associate with AR signaling in CRPC, we investigated the impact of CBP and p300 knockdown on AR signaling in cell line models of CRPC. We determined the impact of individual (CBP or p300) and combined CBP and p300 knockdown by siRNA for 72 hours, studying AR-FL and AR-V7 expression, C-MYC expression, KLK3 expression, and AR signaling in 22Rv1 (Fig. 2A–C) and LNCaP95 (Fig. 2D–F) cells. In both the castration-resistant, AR-SV expressing models 22Rv1 (Fig. 2A and B) and LNCaP95 (Fig. 2D and E), knockdown of p300 and combined CBP and p300 knockdown reduced C-MYC protein expression, KLK3 protein expression, and multiple AR-driven transcripts (*KLK2, KLK3, FKBP5*, and *TMPRSS2*) more than CBP knockdown alone. Consistent with our knockdown experiments, pharmacologic inhibition of p300/CBP suppressed C-MYC expression in models of multiple myeloma (45). Next, to determine whether the impact of CBP

Figure 1. CBP and p300 expression and association with AR activity and acquired endocrine resistance in primary and castration-resistant prostate cancer. **A–D,** Association between primary prostate cancer (PC) CBP (**A**), mCRPC CBP (**B**), primary prostate cancer p300 (**C**), and mCRPC p300 (**D**) expression levels with AR signature from either primary prostate cancer expression data from The Cancer Genome Atlas (TCGA; **A**, **C**; $n = 550$) or Stand Up To Cancer/Prostate Cancer Foundation (SU2C/PCF) mCRPC expression data (**B**, **D**; $n = 120$). *r* values and *P* values are shown and were calculated using Spearman correlation. **E–H,** Association between primary prostate cancer CBP (**E**), mCRPC CBP (**F**), primary prostate cancer p300 (**G**), and mCRPC p300 (**H**) expression levels with acquired ADT resistance signature from either TCGA primary prostate cancer expression data (**E**, **G**; $n = 550$) or SU2C/PCF mCRPC expression data (**F**, **H**; $n = 120$). *r* values and *P* values are shown and were calculated using Spearman correlation. **I,** SU2C/PCF mCRPC transcriptome analyses of RNA-sequencing data from 120 patient biopsies for CBP, p300, and AR expression divided into very high (upper 25% expressed genes), medium high (50%–75% expressed genes), medium low (25%–50% expressed genes), and very low (lower 25% expressed genes). **J,** Nuclear protein expression (H-score) of CBP and p300 in 43 matched, same patient, CSPC (gray) and CRPC (red). Median H-score and interquartile range is shown. *P* values were calculated using Wilcoxon matched-pair signed rank test. **K** and **L,** Representative micrographs of CBP and p300 detection by IHC in matched, same patient, CSPC and CRPC biopsies. Needle biopsies (NB), prostatectomies (prost), bone biopsies (bone), and lymph node biopsies (LN) are shown. Scale bar, 50 μm.

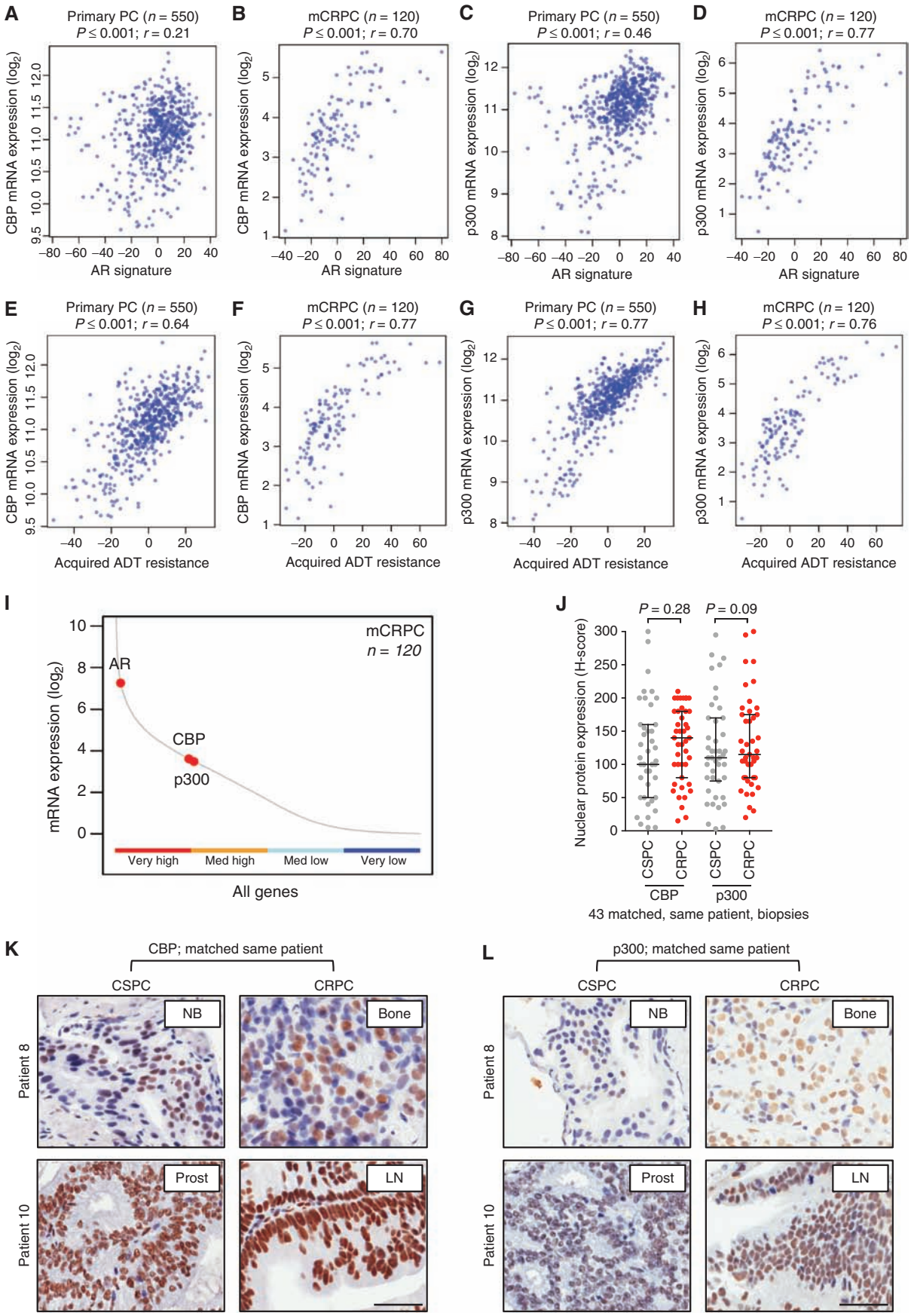

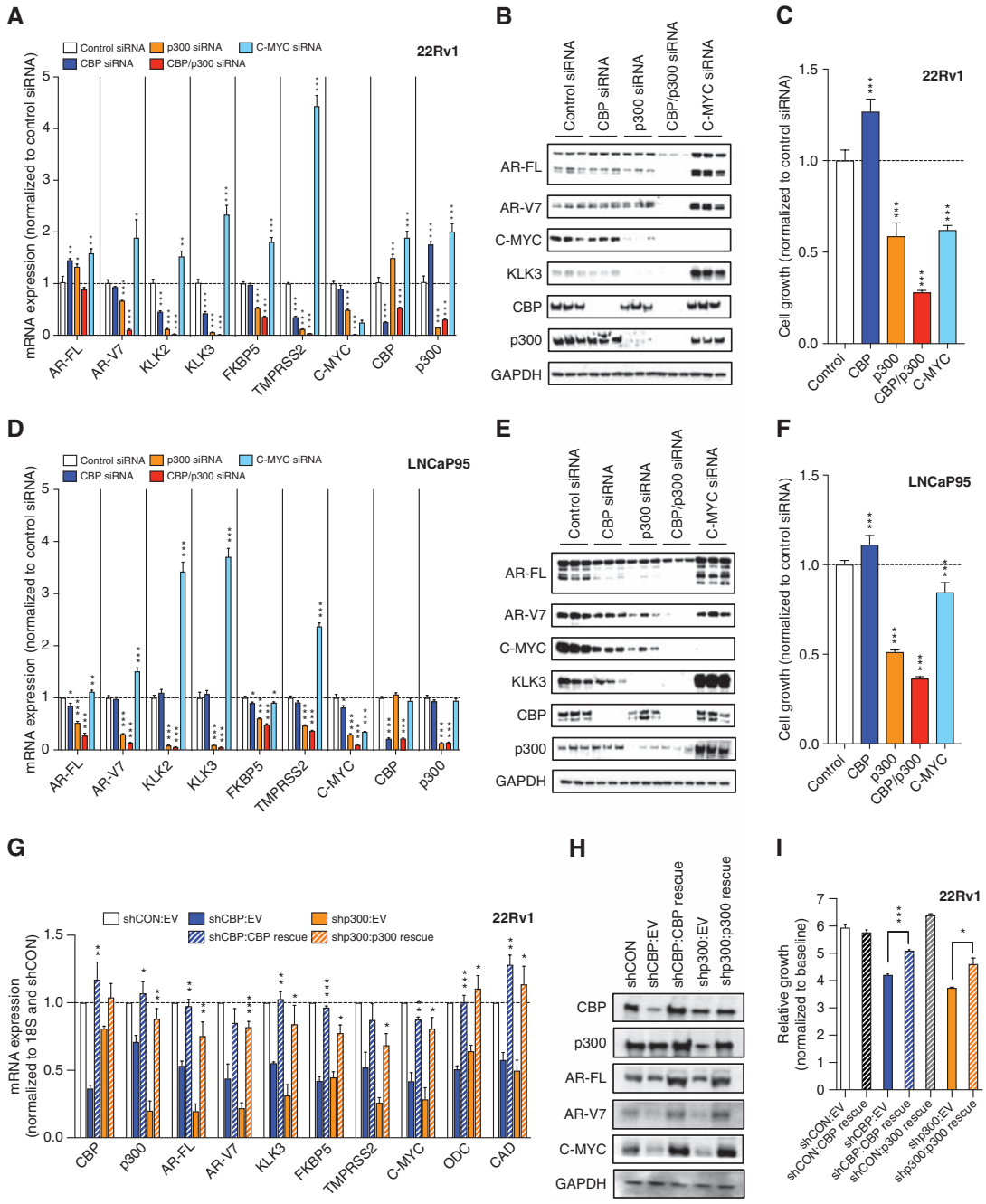

Figure 2. CBP and p300 protein knockdown affects AR-V7 expression and AR signaling independent of C-MYC expression in CRPC models. **A–F,** 22Rv1 (**A–C**) and LNCaP95 (**D–F**) were transfected with a total of 100 nmol/L siRNA with 50 nmol/L of either CBP, p300, p300 plus CBP, or C-MYC siRNA (made up to total with Control siRNA) for 72 hours. The effect of each condition on *AR-FL, AR-V7, KLK2, KLK3, FKBP5, TMPRSS2, C-MYC, CBP*, and *p300* mRNA expression (22Rv1, **A**; LNCaP95, **D**) and AR-FL, AR-V7, C-MYC, KLK3, CBP, p300, and GAPDH protein expression was determined (22Rv1, **B**; LNCaP95, **E**). Mean mRNA expression (normalized to an average of *B2M/GAPDH/HPRT1* and control siRNA; defined as 1.0) with standard error of mean from three individual experiments is shown. Growth assays by CellTiter-Glo were carried out (22Rv1, **C**; LNCaP95, **F**; normalized to control siRNA; defined as 1.0) with standard deviation of an individual experiment with six replicates is shown. *P* values (*, $P \le 0.05$; **, $P \le 0.01$; ***, $P \le 0.001$) were calculated for each condition compared with control siRNA (at equivalent concentration) using unpaired Student *t* test. Western blots are shown in triplicate. **G–I,** 22Rv1 cells with doxycycline-inducible shRNA to Control (shCON), CBP (shCBP), or p300 (shp300) were treated with 10 ng/μg doxycycline for 48 hours prior to transfection with empty vector plasmid (EV), CBP plasmid (CBP rescue), or p300 plasmid (p300 rescue). The effect of each condition on *CBP, p300, AR-FL, AR-V7, KLK3, FKBP5, TMPRSS2, C-MYC, ODC*, and *CAD* mRNA expression (**G**) and CBP, p300, AR-FL, AR-V7, C-MYC, and GAPDH protein expression (**H**) was determined after 48 hours. Mean mRNA expression (normalized to 18S and shCON:EV; defined as 1.0) with standard error of mean from three individual experiments is shown. *P* values (*, $P \le 0.05$; **, $P \le 0.01$; ***, $P \le 0.001$) were calculated for shCBP:EV compared with shCBP:CBP rescue, and shp300:EV compared with shp300:p300 rescue, using unpaired Student *t* test. Western blots demonstrate single experiment. The effect of each condition on relative growth was determined after 5 days using the PicoGreen dsDNA assay (**I**). Mean relative growth (normalized to baseline and shCON:EV; defined as 1.0) with standard error of mean from three individual experiments is shown. *P* values (*, $P \le 0.05$; **, $P \le 0.01$; ***, $P \le 0.001$) were calculated for shCBP:EV compared with shCBP:CBP rescue, and shp300:EV compared with shp300:p300 rescue, using unpaired Student *t* test.

and p300 on AR signaling was through a C-MYC–dependent mechanism, we analyzed C-MYC knockdown in 22Rv1 and LNCaP95 cells; C-MYC knockdown increased AR-FL and AR-V7 protein expression and increased expression of AR-regulated genes, as previously described (Fig. 2A, B, and D–E; ref. 44). Consistent with the impact of p300, and combined CBP and p300 knockdown on AR signaling, these approaches inhibited the growth of 22Rv1 and LNCaP95 cells to a greater extent than CBP and C-MYC knockdown (Fig. 2C and F). The impact of CBP and p300 knockdown on AR and C-MYC signaling was confirmed in both 22Rv1 and the CRPC cell line C4-2, using doxycycline-inducible shRNA (Fig. 2G–I; Supplementary Fig. S3A–S3C). Induction of CBP and p300 shRNA for 48 hours led to reduced protein expression in 22Rv1 (Fig. 2H) and C4-2 (Supplementary Fig. S3B) and associated suppression of downstream targets of AR and C-MYC (Fig. 2G; Supplementary Fig. S3A). Critically, reexpression of CBP and p300 protein following CBP and p300 knockdown led to reactivation of AR and C-MYC signaling and, in part, rescued the growth of 22Rv1 and C4-2 cells (Fig. 2G–I; Supplementary Fig. S3A–S3C). Although some differences were seen between siRNA and shRNA, which are likely in part due to the different methods utilized, the data clearly implicate CBP and p300 as critical regulators of AR signaling and cell proliferation, with this activity being independent of C-MYC in these models of CRPC.

CCS1477 Binds to CBP and p300 Bromodomains with High Affinity and Selectivity

CCS1477 was developed as a potent, selective, and orally bioavailable inhibitor of the conserved bromodomain of p300 and CBP (Fig. 3A). In a surface plasmon resonance (SPR) assay, CCS1477 binds to p300 and CBP with K_d values of 1.3 and 1.7 nmol/L, respectively, and with 170/130-fold selectivity compared with BRD4 with a K_d of 222 nmol/L (Fig. 3B). CCS1477 binding to cellular histones in an in-cell BRET assay gave an IC_{50} of 19 nmol/L for p300 and 1,060 nmol/L for BRD4. In a bromoscan assay of 32 bromodomains (Supplementary Table S4), CCS1477 had only minimal binding to BRD2, 3, 4, 9, and WDR9 (14%–33% of control at 1 μmol/L); there was also no biochemical inhibitory activity in a screen of 97 kinases (Supplementary Table S5), and a safety screen of 44 receptors, enzymes, and ion channels (Supplementary Table S6) at 10 μmol/L (data not shown). Following this characterization of CCS1477, a number of prostate cancer cell lines representative of hormone-dependent and CRPC were treated with CCS1477 at a range of concentrations. The most potent growth-inhibitory activity of CCS1477 was observed in VCaP, 22Rv1, and LNCaP95 (all IC_{50} < 100 nmol/L) that express both AR-FL and AR-V7. In contrast, CCS1477 had less impact on the growth of AR-negative, hormone-independent cell lines (IC_{50} > 1,000 nmol/L; Fig. 3C). These data were further independently validated in the CRPC cell line C4-2 (Supplementary Fig. S4A).

CCS1477 Treatment Induces Significant Transcriptional Alterations, Distinct from BRD4 Inhibition

Next, the CRPC cell line 22Rv1 was selected to investigate the impact of CCS1477 treatment on its transcriptome through RNA sequencing (at derived IC_{50}; 96 nmol/L, Fig. 3D). Importantly, principal component analyses (PCA) suggested a high level of concordance between biological replicates as shown in sample clustering within treatment groups (Supplementary Fig. S4B). Significant transcriptional alterations were identified after drug treatment, with 3,406 transcripts induced and 3,262 repressed (Supplementary Fig. S4C). To investigate pathways associated with the gene-expression changes seen, gene set enrichment analysis (GSEA) was performed using the Hallmarks gene set from the Molecular Signatures Database (MSigDB; refs. 46, 47). Few pathways displayed enrichment after CCS1477 treatment, with those identified relating mainly to cell-cycle– and DNA-repair–related pathways (Fig. 3E); critically, those with attenuated enrichment after CCS1477 treatment included androgen response and MYC target pathways, validating p300/CBP knockdown data and further implicating these in modulating these key prostate cancer signaling pathways (Fig. 3E).

Having demonstrated CCS1477 selectivity for p300 and CBP over BRD4 in SPR analysis, we next compared the transcriptional impact of a known BET inhibitor (JQ1) on transcriptomic profiling in 22Rv1 cells (Supplementary Fig. S4B). Interestingly, samples treated with JQ1 or CCS1477 displayed a high degree of separation after PCA, suggesting that these samples have distinct transcriptional alterations after drug treatment (Supplementary Fig. S4B). Further supporting this concept, differential expression analyses in JQ1-treated cells resulted in a significant increase in altered transcripts when compared with CCS1477-treated cells (Supplementary Fig. S4C and S4D). In order to determine downstream pathways driven by gene-expression events after drug treatment, GSEA was performed (Supplementary Fig. S4E). Interestingly, although a number of pathways were identified after either drug treatment, CCS1477 treatment was associated with an increased number of altered pathways compared with JQ1, suggesting that although CCS1477 affected a smaller repertoire of gene-expression changes compared with JQ1, these were highly coordinated to affect specific pathways. Furthermore, CCS1477 GSEA was exclusively associated with de-enrichment of the androgen response pathway, further supporting a key role for p300/CBP in regulating this pathway in prostate cancer.

Finally, having shown that CCS1477 and JQ1 affect distinct transcriptional changes in CRPC cells, we explored whether CCS1477 could overcome acquired resistance to JQ1 therapy. JQ1-resistant 22Rv1 cells were generated by culture in the presence of increasing concentrations of JQ1, or vehicle, over the course of 6 months, and then confirmed (parental vs. resistant IC_{50}; 60 vs. 7,300 nmol/L; Supplementary Fig. S4F) with resistance to multiple BET inhibitors (JQ1, OTX-015, I-BET151; all > 100-fold). Importantly, consistent with distinct transcriptional changes, JQ1-resistant 22Rv1 cells were more sensitive to CCS1477 treatment, confirming the selectivity of this p300 and CBP inhibitor being distinct from that of BRD4 inhibitors (Supplementary Fig. S4F). Taken together, these data demonstrate CCS1477 as a potent, and selective, inhibitor of the bromodomains of CBP and p300, with the ability to regulate prostate cancer growth and key prostate cancer signaling pathways, distinct from BRD4 inhibition.

A

CCS1477

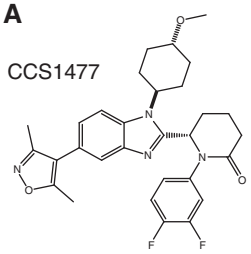

B

	k_{on} ($M^{-1}s^{-1}$)	SE ($M^{-1}s^{-1}$)	k_{off} (s^{-1})	SE (s^{-1})	K_D (nmol/L)	SE (nmol/L)	t ½ (sec)
p300	1.1×10^6	1.2×10^5	1.9×10^4	1.2×10^4	1.3	0.2	527
CBP	1.4×10^6	1.3×10^5	3.1×10^3	1.7×10^4	1.7	0.2	322
BRD4	7.2×10^5	6.1×10^4	1.5×10^1	1.0×10^2	222	25.1	6.6

C

Cell line	AR status	Model	IC_{50} (nmol/L)
LNCaP	AR-FL	Hormone dependent	230
LNCaP-AR	AR-FL (overexpressed)	CRPC	150
VCaP	AR-FL/SV	CRPC	50
22Rv1	AR-FL/SV	CRPC	96
LNCaP95	AR-FL/SV	CRPC	86
DU145	AR negative	Hormone independent	1,280
PC3	AR negative	Hormone independent	1,490

D

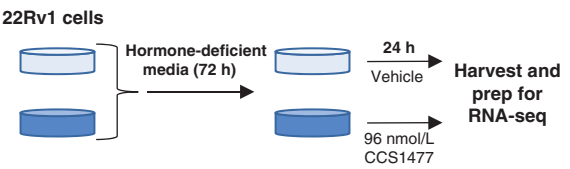

E

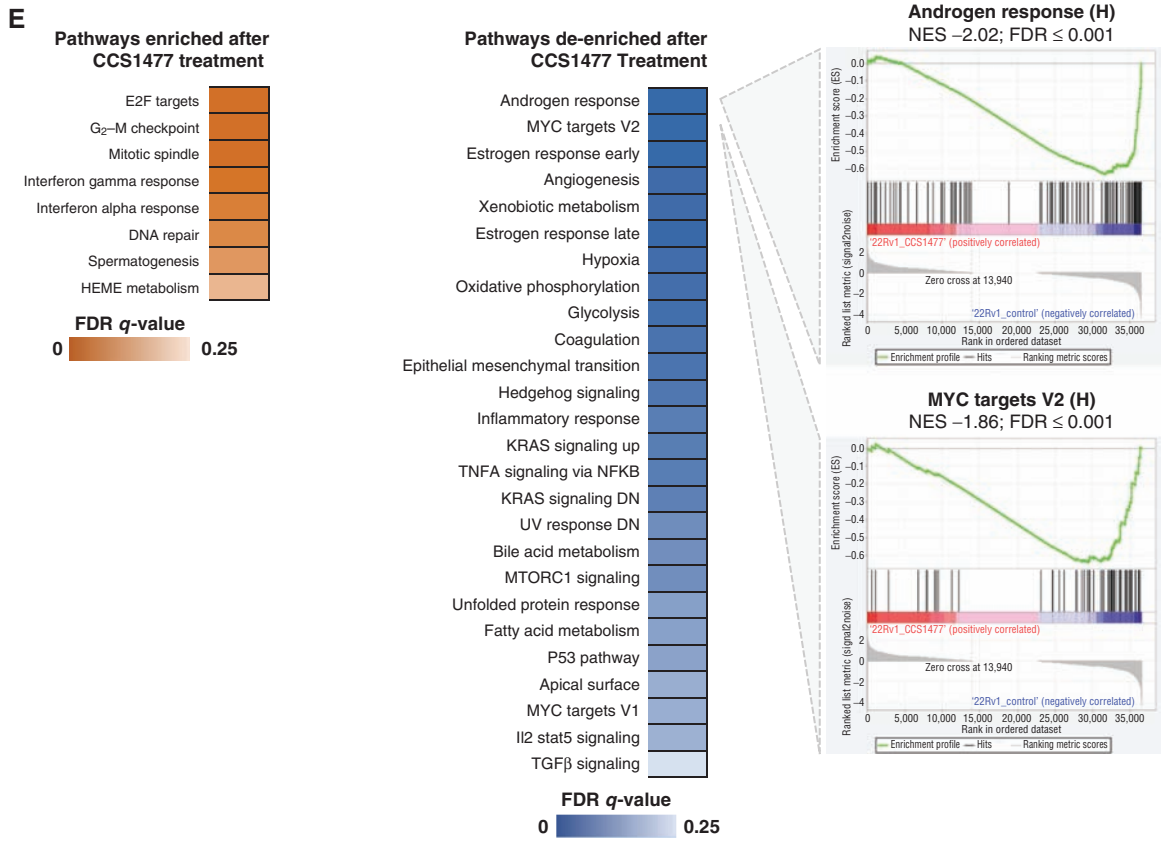

Figure 3. CCS1477, a selective p300/CBP inhibitor, downregulates AR and C-MYC signaling and inhibits the growth of prostate cancer models. **A,** Chemical structure of CCS1477. **B,** A summary of the derived kinetic parameters from analysis of CCS1477 in an SPR assay (K_{on} is the rate constant for the association of the protein–ligand reaction; SE, standard error of the mean; K_{off} is the rate constant for the dissociation of the protein–ligand reaction; K_d is the equilibrium constant for the dissociation equilibrium; $T_{1/2}$ is the half-life of the protein–ligand reaction). **C,** Inhibition of cell proliferation by CCS1477 in prostate cancer cell lines representative of hormone dependent, hormone independent, or CRPC with the IC_{50} determined by either CellTiter-Glo or CyQuant. **D,** Schematic of RNA-sequencing experimental setup. Briefly, 22Rv1 cells were grown in hormone-deficient media for 72 hours prior to treatment with CCS1477 (96 nmol/L) or vehicle control. RNA sequencing was performed in biological triplicate. **E,** Gene set enrichment analysis using the hallmarks pathway from the Molecular Signatures Database [false discovery rate (FDR) < 0.25]. Briefly, normalized RNA-sequencing counts were queried for overrepresented pathways with enrichment (left) and de-enrichment (right) after CCS1477 treatment are shown. Leading-edge plots for the top two de-enriched pathways after CCS1477 treatment are shown. Normalized enrichment score (NES) and FDR are shown.

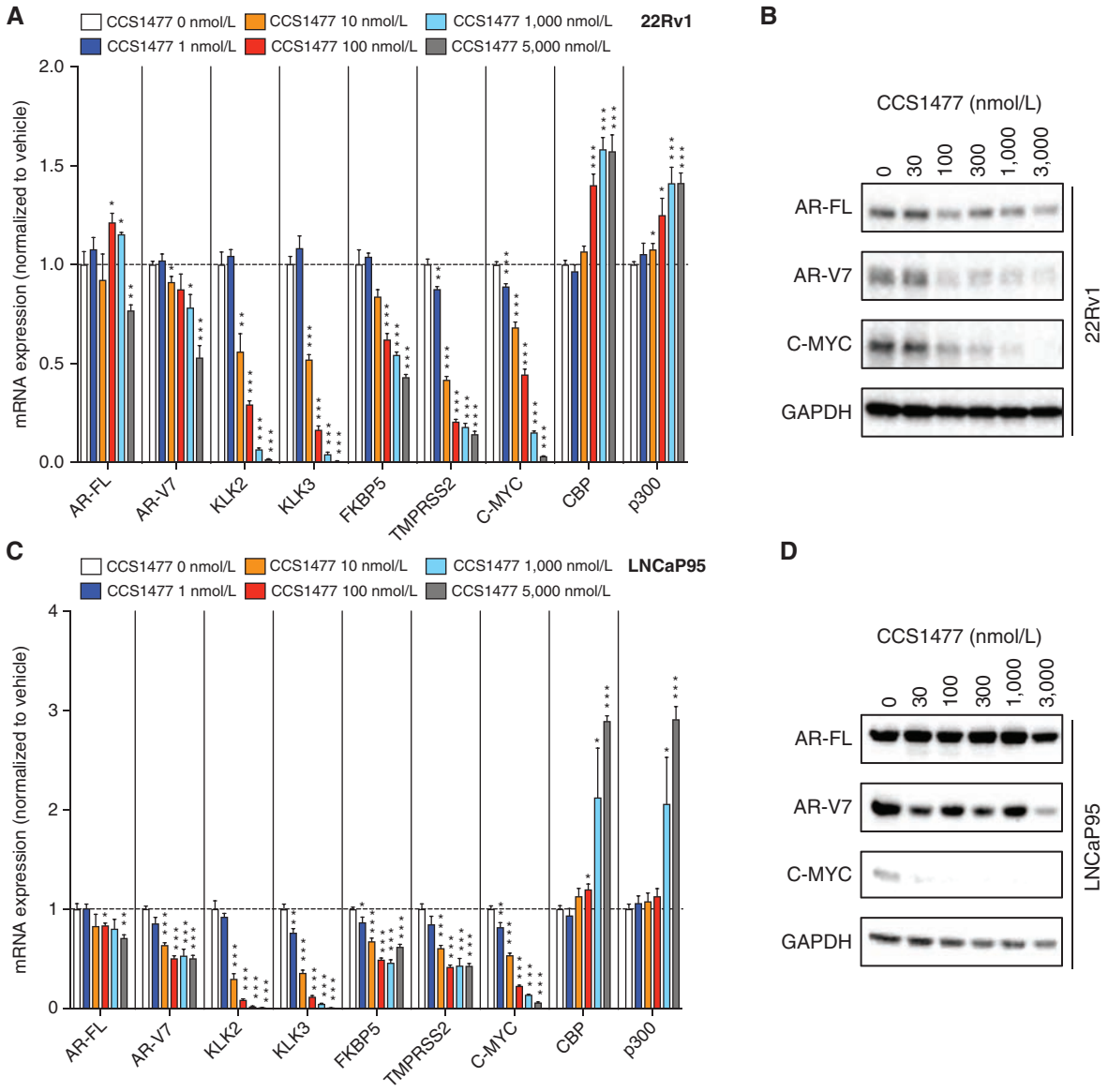

Figure 4. CCS1477 inhibits AR and C-MYC signaling in cell line models of CRPC. **A–D,** 22Rv1 (**A** and **B**) and LNCaP95 (**C** and **D**) were treated with vehicle (0 nmol/L = DMSO 0.1%) or various concentrations of CCS1477 (1, 10, 30, 100, 300, 1,000, 3,000 or 5,000 nmol/L) for 48 hours (72 hours for **B**). The effect of each condition on *AR-FL, AR-V7, KLK2, KLK3, FKBP5, TMPRSS2, C-MYC, CBP*, and *p300* mRNA expression (22Rv1, **A**; LNCaP95, **C**) and AR-FL, AR-V7, C-MYC, and GAPDH protein expression was determined (22Rv1, **B**; LNCaP95, **D**). Mean mRNA expression (normalized to an average of *B2M/GAPDH/HPRT1* and control siRNA; defined as 1.0) with standard error of mean from three individual experiments is shown. *P* values (*, $P \le 0.05$; **, $P \le 0.01$; ***, $P \le 0.001$) were calculated for each treatment condition compared with vehicle using unpaired Student *t* test. Single representative Western blot shown from three separate experiments. (*continued on next page*)

CCS1477 Inhibits AR Signaling in Cell Line Models of CRPC Expressing AR Splice Variants

Having shown that CCS1477 affects AR and C-MYC signaling in 22Rv1 cells, we next further evaluated the impact of CCS1477 on AR and C-MYC signaling across multiple cell line models of CRPC. 22Rv1, LNCaP95, and C4-2 cells were treated with increasing concentrations of CCS1477 for longer (48 hours; 22Rv1 and LNCaP95; Fig. 4A–D) or shorter (16 hours; 22Rv1 and C4-2; Supplementary Fig. S5A and S5B) exposures, and the impact on AR-FL and AR-V7 expression, C-MYC expression, and downstream AR and C-MYC signaling was determined. CCS1477 reduced expression of AR-regulated genes (*KLK2, KLK3*, and *TMPRSS2*) in both 22Rv1 and LNCaP95 cells at 48 hours (Fig. 4A and C). CCS1477 also reduced C-MYC protein expression in both 22Rv1 and LNCaP95 cells and AR-V7 protein expression in 22Rv1 cells, without clear impact on AR-FL protein expression in 22Rv1 and LNCaP95 cells (Fig. 4B and D). In addition, CCS1477 reduced C-MYC mRNA and downstream AR and C-MYC signaling in 22Rv1 and C4-2 cells at 16 hours (Supplementary Fig. S5A and S5B). Interestingly, there was also a more marked effect on AR

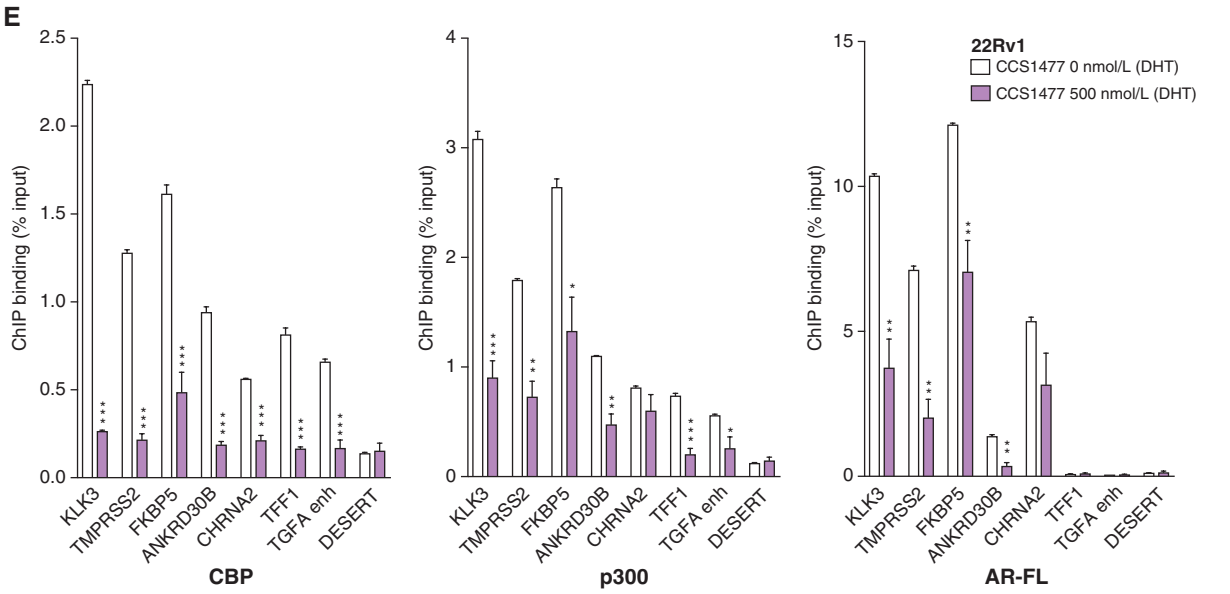

Figure 4. ***(Continued)*** **E,** 22Rv1 cells were plated in hormone-deficient media for 72 hours. Thereafter, cells were treated with vehicle (0 nmol/L = DMSO 0.1%) or CCS1477 500 nmol/L for 8 hours, with 10 nmol/L dihydrotestosterone (DHT) being added 3 hours before harvest. ChIP was performed with CBP, p300, and AR-FL antibodies, followed by PCR with primers designed for known AR binding sites whose gene expression was significantly downregulated by CCS1477 treatment (*KLK3, TMPRSS2, FKBP5 ANKRD30B*, and *CHRNA2*), and to known CBP binding sites [*TFF1* and *TGFA* enhancer (enh)]. Mean binding as percentage input with standard error of mean from three individual experiments is shown. *P* values (*, $P \leq 0.05$; **, $P \leq 0.01$; ***, $P \leq 0.001$) were calculated for vehicle compared with CCS1477 treatment using unpaired Student *t* test.

transcript at 16 hours, compared with 48 hours, which may be a time-dependent effect with apparent increase over time (Supplementary Fig. S5C). Interestingly, treatment with CCS1477 at the highest concentrations tested led to increased expression of CBP and p300 mRNA (Fig. 4A and C). We next determined whether CCS1477 affected the recruitment of CBP, p300, and AR-FL to known AR binding sites whose gene expression was significantly downregulated by CCS1477 treatment (*KLK3, TMPRSS2, FKBP5 ANKRD30B*, and *CHRNA2*) and to known CBP binding sites (*TFF1* and *TGFA* enhancer; refs. 48, 49). 22Rv1 and C4-2 cells were treated with 500 nmol/L CCS1477 or vehicle (5 hours) prior to stimulation with 10 nmol/L dihydrotestosterone (3 hours) and the impact on CBP, p300, and AR-FL recruitment to identified binding sites was determined by chromatin immunoprecipitation (ChIP; Fig. 4E; Supplementary Fig. S5D). Interestingly, CCS1477 reduced the recruitment of CBP, p300, and AR-FL to those AR binding sites whose gene expression was downregulated in response to CCS1477 treatment in both 22Rv1 and C4-2 cells (Fig. 4E; Supplementary Fig. S5D). Furthermore, CCS1477 reduced the recruitment of CBP and p300 to known CBP binding sites in both cell lines, with low levels of AR-FL found at both these sites (Fig. 4E; Supplementary Fig. S5D). Taken together, these data suggest that CCS1477 regulates AR signaling by affecting the recruitment of CBP, p300, and AR-FL to known AR binding sites, and has the potential to abrogate persistent AR signaling in CRPC.

CCS1477 Inhibits Tumor Growth and AR Signaling in a 22Rv1 Mouse Xenograft Model

Having demonstrated that CCS1477 inhibits AR and C-MYC signaling and prostate cancer cell growth, we sought to determine if CCS1477 inhibited the growth of 22Rv1 mouse xenografts. We first evaluated, in a mouse pharmacokinetic study, the time course of CCS1477 and exposure relationship to *in vitro* cell proliferation and binding characteristics (Supplementary Fig. S6A). A single oral dose of 30 mg/kg resulted in free blood concentrations (corrected for protein binding) that were in excess of the 22Rv1 cell line proliferation IC_{50} (96 nmol/L) and the p300 in-cell binding IC_{50} (19 nmol/L, NanoBRET) for 10 hours. At no time did the free blood concentrations approach the in-cell binding IC_{50} for BRD4 (1,060 nmol/L). In 22Rv1 mouse xenografts, oral dosing with CCS1477 significantly ($P \leq 0.001$) affected tumor growth at 10 mg/kg daily (QD), 20 mg/kg QD, and 30 mg/kg every other day (QOD; Fig. 5A). All doses tested were well tolerated with no change in body weight or condition of the animals (data not shown). Interestingly, despite treatment being stopped after 28 days, tumor growth inhibition was sustained until day 52, when the study was terminated (Fig. 5A); there were no detectable levels of CCS1477 in plasma or tumor at this time (data not shown). The effects of CCS1477 on AR-FL, AR-V7, and C-MYC protein expression, and AR-regulated genes (*KLK3* and *TMPRSS2*) were examined in tumors collected at days 7, 28, and 52 (Fig. 5B, C and E; Supplementary Fig. S6B and S6C). After 7 days of treatment, CCS1477 had reduced AR-FL, AR-V7, and C-MYC protein expression, at all doses tested (Fig. 5C). In addition, *TMPRSS2* but not *KLK3* gene expression was reduced (Fig. 5B). At the end of the treatment period at day 28, AR-FL and AR-V7 protein expression was reduced in all dosing groups, as was C-MYC at the 30 mg/kg QOD dosing group (Fig. 5C). In addition, *TMPRSS2* gene expression continued to be suppressed by CCS1477 at day 28, and at this time point the

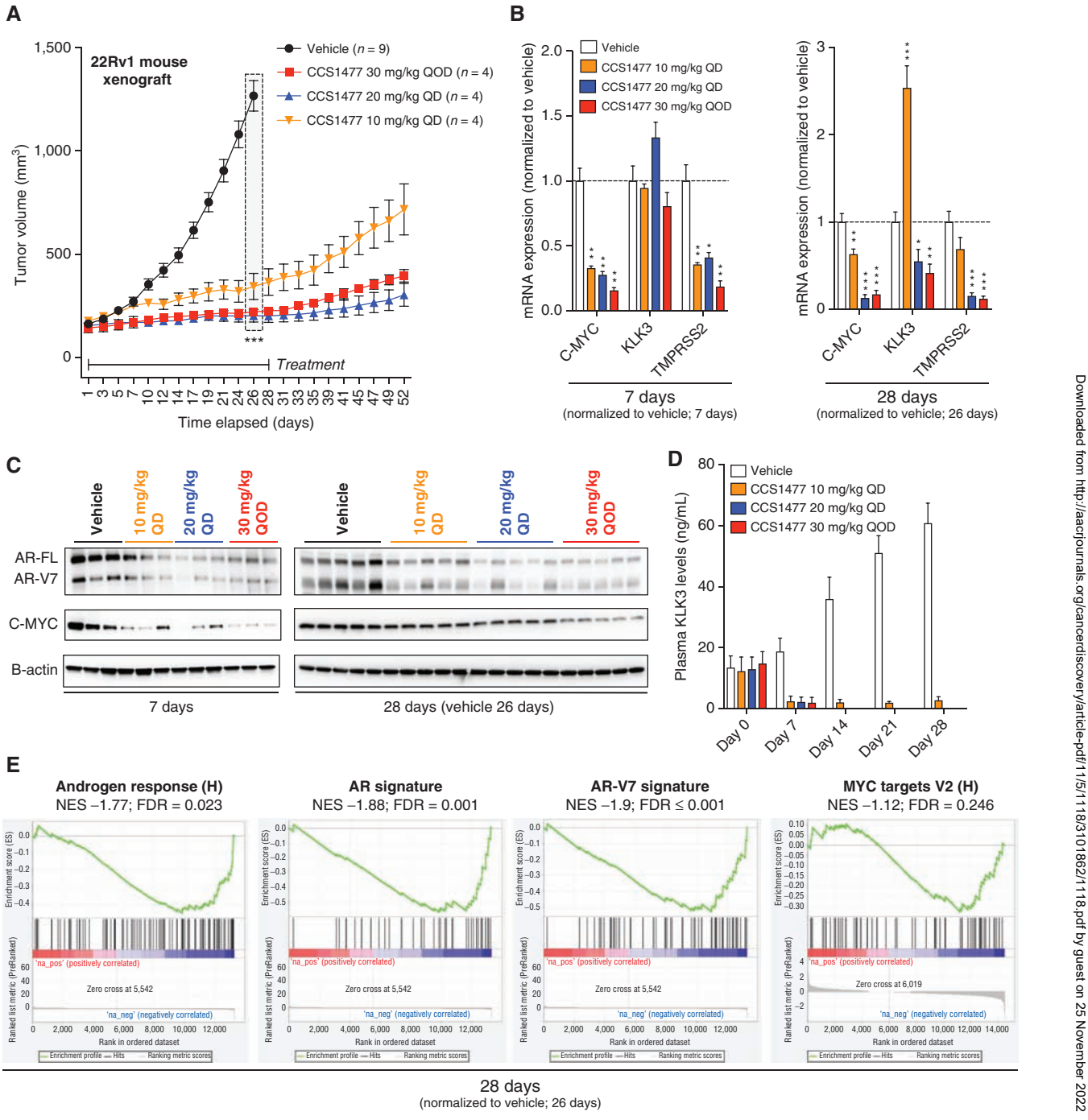

Figure 5. CCS1477 decreases AR and AR-V7 signaling and inhibits growth in a 22Rv1 mouse xenograft model. **A,** Once 22Rv1 xenograft tumor volume reached 150 mm^3, treatment commenced with either vehicle (measurements for $n = 9$) or CCS1477 (measurements for $n = 4$ per group), administered by oral gavage, at 10 or 20 mg/kg daily (QD) or at 30 mg/kg every other day (QOD) for 28 days (vehicles collected at 26 days due to reaching a legal maximum). Mean tumor volume with standard error of mean is shown. *P* values (*, $P \le 0.05$; **, $P \le 0.01$; ***, $P \le 0.001$) were calculated for vehicle compared with CCS1477 at 10 mg/kg daily, 20 mg/kg daily, and 30 mg/kg QOD at 26 days using unpaired Student *t* test. **B,** The effect of each condition on C-MYC, KLK3, and TMPRSS2 mRNA expression was determined for 7 days (left) and 28 days (26 days for vehicle; right). Mean mRNA expression (normalized to an average of GAPDH/RPLP0 and vehicle treatment; defined as 1.0) with standard error of mean from individual tumors in each group (3 per group in 7 days, 5 per group from 28 days) are shown. *P* values (*, $P \le 0.05$; **, $P \le 0.01$; ***, $P \le 0.001$) were calculated for each treatment condition compared with vehicle using unpaired Student *t* test. **C,** The effect of each condition on AR-FL, AR-V7, C-MYC, and beta-actin protein expression was determined for 7 days (left) and 28 days (26 days for vehicle; right). **D,** Blood plasma KLK3 protein levels (ng/mL) were determined every 7 days by ELISA. Mean KLK3 protein levels with standard deviation from mice in each treatment group are shown. **E,** Gene set enrichment analysis of RNA sequencing for 26 days vehicle group and 28 days 20 mg/kg CCS1477 daily group comparing the androgen response (left), AR signature (center), and AR-V7 signature (right) with normalized enrichment score (NES) and FDR are shown.

20 mg/kg QD and the 30 mg/kg QOD doses decreased *KLK3* gene expression (Fig. 5B). At day 52, after 24 days without CCS1477 treatment, all protein biomarkers had returned to control levels but there was prolonged reduction in *KLK3* and *TMPRSS2* gene expression, particularly at the 30 mg/kg QOD dose (Supplementary Fig. S6B and S6C). In addition to tumor pharmacodynamic analyses, plasma KLK3 levels increased in the vehicle group between days 0 and 28, reflecting the increase in tumor volume during this time (Fig. 5D). Treatment with CCS1477 at all doses caused a decrease in the plasma KLK3 concentrations (Fig. 5D). Finally, RNA-sequencing analysis of tumors treated with 20 mg/kg QD for 28 days demonstrated de-enrichment of signatures of AR and AR-V7 signaling when compared with vehicle, with the AR response pathway identified as one of the top de-enriched pathways (Fig. 5E; Supplementary Table S7). Although there was a trend toward de-enrichment of MYC targets, in contrast to the 22Rv1 cell line experiments, this was not significant (Fig. 5E). Taken together, these data demonstrate that inhibition of CBP and p300 by CCS1477 suppresses growth of a 22Rv1 mouse xenograft model with associated reduction in AR signaling.

CCS1477 Inhibits Tumor Growth and AR Signaling in a Patient-Derived Model of Treatment-Resistant Lethal Prostate Cancer

We next investigated CCS1477 in a patient-derived model of treatment-resistant lethal prostate cancer, utilizing a patient-derived xenograft (PDX; CP50) resistant to enzalutamide treatment that has an amplified *AR* and expresses AR-V7 as well as amplified *AKT2* and *C-MYC* (44). CP50 PDX was derived from the lymph node biopsy of a patient with CRPC that had progressed through all standard-of-care treatments and was further passaged in castrate mice to develop CP50c PDX (Fig. 6A). Because 20 mg/kg CCS1477 QD had blocked tumor growth with pharmacodynamic studies indicating AR signaling regulation in 22Rv1 mouse xenografts, this dose and schedule was explored in the CP50c PDX. CP50c PDX were treated orally with 20 mg/kg CCS1477 QD, or vehicle, continuously until tumors exceeded the legal limit (Fig. 6B). Treatment of CP50c with CCS1477 significantly ($P = 0.02$) reduced tumor growth when compared with vehicle (Fig. 6C), and significantly ($P \leq 0.001$) prolonged survival (time to 300% growth; Fig. 6D). At 8 days, CCS1477 QD decreased C-MYC gene and protein expression but had limited impact on AR-FL and AR-V7 protein expression, or on *KLK3* and *TMPRSS2* gene expression, when compared with vehicle (Fig. 6E and F). In contrast, RNA-sequencing analysis of tumors treated with 20 mg/kg CCS1477 QD for 8 days demonstrated de-enrichment of signatures of AR and AR-V7 signaling when compared with vehicle (Fig. 6G). Consistent with this, the AR response pathway was identified as one of the top downregulated pathways, along with other pathways, including MYC targets, important for prostate cancer progression (Fig. 6G; Supplementary Table S8). These data show that CCS1477 inhibits AR signaling and tumor growth in advanced, treatment-resistant CRPC.

CCS1477 Modulates Plasma KLK3 Levels and Regulates Key Prostate Cancer Therapeutic Targets in Patients with Advanced Prostate Cancer

CCS1477 has now entered a first-in-human phase I trial (NCT03568656). We next determined whether CCS1477 recapitulated the preclinical data presented in patients with mCRPC treated on this trial. We investigated plasma KLK3 levels and pharmacodynamic regulation of specific proteins (AR-FL, AR-V7, C-MYC, KLK3, CBP, p300, and Ki-67) by IHC in two patients treated with CCS1477 in the dose-escalation phase of this ongoing clinical trial. C-MYC antibody specificity for IHC was confirmed using siRNA knockdown in HeLa cells (Supplementary Fig. S7A). Patient 1 was administered 50 mg CCS1477 BD on a 3-day-on and 4-day-off schedule (Fig. 7A); he had an initial fall in plasma KLK3, which then stabilized (Fig. 7A); study of predose and postdose biopsies (4 hours after CCS1477 dose) demonstrated a reduction in AR-V7 and C-MYC protein expression (Fig. 7B and C), but no change in AR-FL, KLK3, CBP, p300, or Ki-67 protein levels (Fig. 7B and C). In contrast, patient 2 was treated with 25 mg CCS1477 BD continuously with plasma KLK3 levels continuing to rise despite this (Fig. 7D), although pre- and postdose (3 hours after CCS1477 dose) biopsy studies demonstrated a postdose reduction in C-MYC and Ki-67 protein expression (Fig. 7E and F) but no change in AR-FL, AR-V7, KLK3, CBP, or p300 protein levels, in keeping with the plasma KLK3 results (Fig. 7E and F). Taken together, these preliminary data suggest that CCS1477 can modulate prostate cancer AR signaling, and consequently plasma KLK3 levels; further analysis of this ongoing phase I study is now required to confirm these observations. Furthermore, the demonstration that

Figure 6. CCS1477 decreases AR and AR-V7 signaling and inhibits growth in a patient- derived model of lethal prostate cancer. **A,** PDX CP50c was developed from lymph node biopsy from a patient who had progressed through all standard-of-care treatments for CRPC. **B,** Schematic overview of CP50c PDX experimental design. Once CP50c PDX tumor volume reached 300 mm^3 treatment, administered by oral gavage, commenced with either vehicle or 20 mg/kg CCS1477 daily (QD) until reaching 300% of starting volume (long term, $n = 6$ per group), with an additional subset treated for short-term analysis at 8 days ($n = 4$ per group for mRNA; $n = 3$ for Western blot). **C** and **D,** Mean growth (normalized to start; defined as 100%) with standard error of mean was determined for each tumor. *P* value (*, $P \leq 0.05$; **, $P \leq 0.01$; ***, $P \leq 0.001$) was calculated for vehicle compared with CCS1477 at 20 mg/kg daily at 31 to 35 days using unpaired Student *t* test. (**C**). Time to reach 300% growth was used as a surrogate endpoint for survival. HR with 95% confidence intervals and *P* values for univariate cox survival model are shown (**D**). **E** and **F,** The effect of 20 mg/kg CCS1477 daily compared with vehicle at 8 days on AR, AR-V7, KLK3, TMPRSS2, and C-MYC mRNA expression (**E**) and on AR- FL, AR-V7, C-MYC, and GAPDH protein expression was determined (**F**). Mean mRNA expression (normalized to an average of B2M/GAPDH/HPRT1 and vehicle treatment; defined as 1.0) with standard error of mean from individual tumors in each group is shown. *P* values (*, $P \leq 0.05$; **, $P \leq 0.01$; ***, $P \leq 0.001$) were calculated for each treatment condition compared with vehicle using unpaired Student *t* test. **G,** Gene set enrichment analysis of RNA sequencing from vehicle group and 20 mg/kg CCS1477 daily group at 8 days comparing the androgen response (left), AR signature (center left), AR-V7 signature (center right), and MYC targets V2 (right) with normalized enrichment score (NES) and FDR presented.

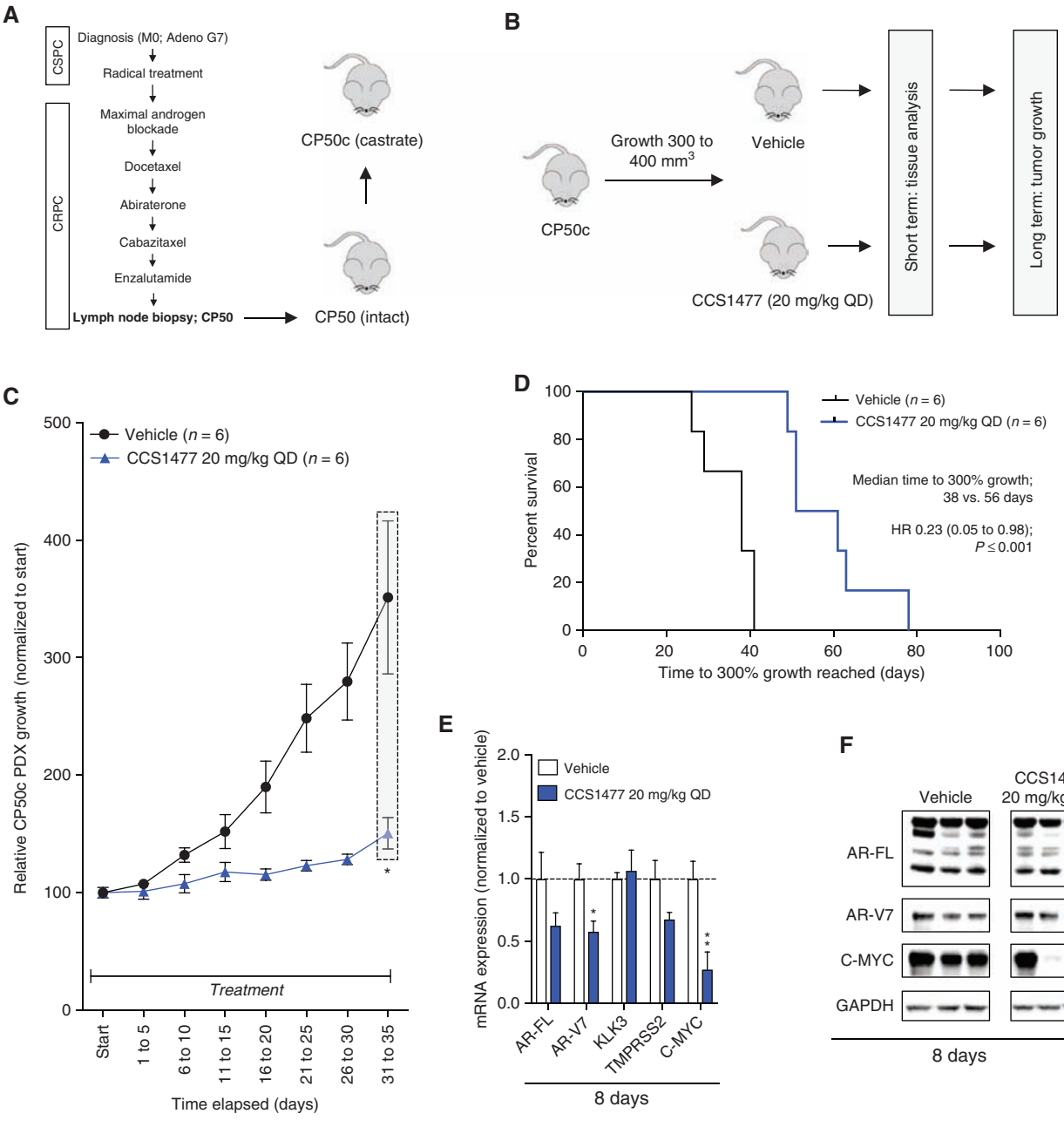

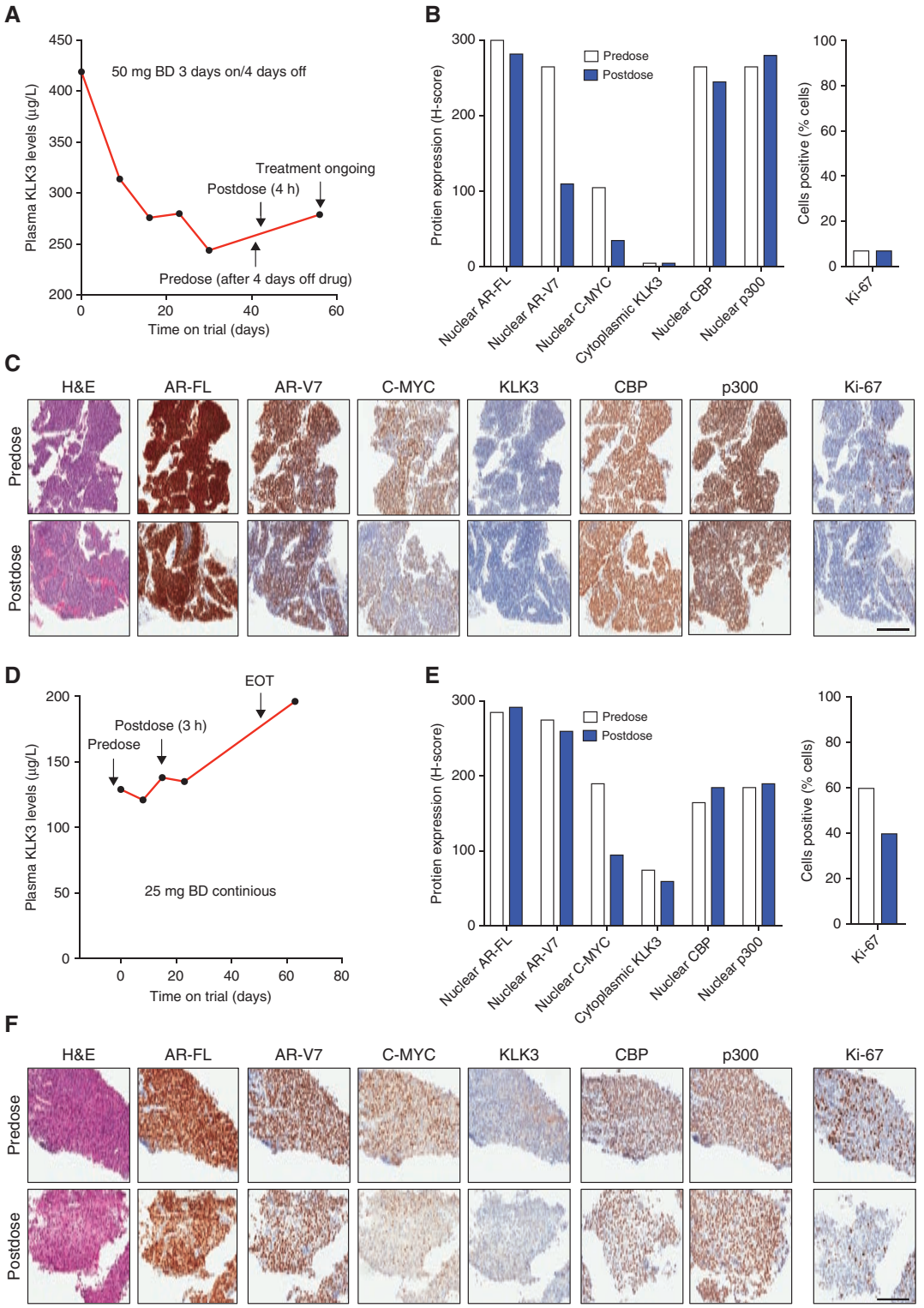

Figure 7. CCS1477 regulates key prostate cancer therapeutic targets and modulates blood KLK3 in patients with CRPC. **A–F,** Patient 1 (**A–C**) and patient 2 (**D–F**) were treated with CCS1477 within an ongoing phase I clinical trial (NCT03568656). Patient 1 (**A–C**) was treated orally with 50 mg twice daily (BD) on a 3-day-on and 4-day-off schedule. Blood KLK3 levels and timing of predose (after 4-day off treatment) and postdose (4-hour post-CCS1477 dose) biopsies are shown (**A**). The patient remains on trial. Quantification (**B**) and representative micrographs for hematoxylin and eosin (H&E), AR-FL, AR-V7, C-MYC, KLK3, CBP, p300, and Ki-67 IHC predose and postdose are shown (**C**). Scale bar, 200 µm. Patient 2 (**D–F**) was treated orally with 25 mg BD continuously. Blood KLK3 levels and timing of predose (prior to starting treatment) and postdose (3 hours after CCS1477 dose) biopsies are shown (**D**). The patient has stopped treatment. Quantification (**E**) and representative micrographs for H&E, AR-FL, AR-V7, C-MYC, KLK3, CBP, p300, and Ki-67 IHC predose and postdose are shown (**F**). Scale bar, 200 µm.

CCS1477 affects AR signaling in models of CRPC suggests it could be utilized in combination with current AR targeting therapies such as enzalutamide. Interestingly, treatment with CCS1477 significantly ($P \leq 0.001$) reduced tumor growth when compared with enzalutamide in the LNCaP-Bic mouse, and although treatment with CCS1477 and enzalutamide in combination further suppressed growth compared with CCS1477 alone, this did not reach statistical significance (Supplementary Fig. S7B). These data suggest that combination therapy with CCS1477 and enzalutamide may merit further exploration.

DISCUSSION

Persistent AR signaling is reported to remain key to driving the growth of most CRPC tumors. Herein we describe studies validating p300 and CBP as prostate cancer therapeutic targets in both CSPC and CRPC. We then report on a novel agent, CCS1477, that inhibits the bromodomain of these paralog proteins that are critical transcriptional coactivators of the AR. We also show that targeting p300 and CBP via their conserved bromodomain can abrogate the downstream oncogenic consequences of persistent AR activation in CRPC, which is functionally distinct from BRD4 inhibition. We first show that p300 and CBP are highly expressed in both CSPC and CRPC clinical samples, with this associating with AR signaling and acquired ADT resistance signatures. The acquired ADT signature represents 49 AR bound genes that do not respond to hormone stimulation, but are differentially regulated as resistance to hormone deprivation evolves *in vitro* (43). In addition, the acquired ADT resistance signature associates with shorter time to biochemical recurrence following prostatectomy, potentially identifying those primary prostate cancers where AR-driven processes are already active and driving tumor progression (43). It is therefore unsurprising that p300 and CBP associate significantly with both AR signaling and acquired ADT resistance signatures. Furthermore, p300 expression associates with shorter time to CRPC, suggesting a potential role in endocrine resistance. Next, we investigated targeting CBP and p300, either separately or in combination, through siRNA and shRNA knockdown in multiple CRPC cell lines and demonstrated consistent reduction in expression of AR-FL, AR-V7, and C-MYC proteins, with associated downregulation of AR and C-MYC regulated transcripts, which is consistent with other studies (34). Moreover, p300, and combined p300 and CBP, knockdown significantly reduced the growth of CRPC cell lines. Furthermore, the reexpression of p300 and CBP led to reactivation of AR and C-MYC signaling and, in part, rescued the growth of 22Rv1 and C4-2 cells. Overall, these data confirm that the CRPC cell lines depend on p300 and CBP, as previously described (34). We also highlight that although C-MYC expression is affected by p300 and CBP reduction, as previously reported, direct targeting of C-MYC with siRNA does not recapitulate the effects of p300 and CBP reduction but conversely increases expression of AR-FL–, AR-V7–, and AR-regulated transcripts, implying that the impact on AR signaling by p300/CBP blockade remains independent of C-MYC (34, 45).

This is the first publication of the chemical structure of CCS1477; we show that it is a potent and selective inhibitor (sparing BRD2/3/4) of the common bromodomain of p300/CBP. Other small-molecule bromodomain inhibitors have been developed that target the BET proteins BRD2, BRD3, and BRD4 (such as JQ1, OTX-015, and I-BET151) and have been evaluated in clinical trials. These can affect AR signaling, but are limited by tolerability issues; BET inhibitors have narrow therapeutic windows due to hematologic toxicity (44, 50, 51). CCS1477 is, however, 170-fold selective over BRD4, with minimal binding to BRD2/3, and demonstrates distinct modulation of transcriptomic profiling and cellular pathways when compared with BET inhibition. Consistent with this, we demonstrate that CCS1477 is active in *in vivo* models at doses resulting in plasma concentrations that are well below the in-cell IC_{50} for BRD4. Collectively, these data indicate that the observed *in vivo* effects are attributable to inhibition of p300/CBP and no involvement of BRD4. We also demonstrate that CCS1477 has antitumor activity against multiple AR/AR-V7–dependent cell lines (LNCaP, LNCaP-AR, VCaP, 22Rv1, LNCaP95, and C4-2) and is less effective against two AR-independent cell lines (DU145 and PC3). In a dose-dependent fashion, CCS1477 recapitulated the siRNA p300/CBP knockdown model, reducing the expression of AR-driven and C-MYC–driven transcripts, consistent with other p300/CBP inhibitors (32). Furthermore, our data show that CCS1477 is likely to inhibit AR signaling through its ability to affect recruitment of CBP, p300 and AR-FL to known AR binding sites and regulate associated gene expression. Although these data are consistent with CCS1477 targeting the bromodomain of CBP and p300, we cannot preclude additional effects of CCS1477 on histone acetylation as previously described in lymphoma cell lines and for an alternative small-molecule inhibitor targeting the bromodomain of CBP and p300 in prostate cancer cell lines (34, 52). It will be important to further understand these underpinning mechanisms as these agents progress through clinical development. Finally, there was a dose-dependent increase in mRNA expression of p300 and CBP in CRPC cell lines after CCS1477 treatment; it will be important to further investigate this, as this may represent a potential mechanism by which therapeutic resistance may occur to such therapies.

We acquired *in vivo* evidence for the antitumor activity of CCS1477. In the 22Rv1 mouse xenograft model, CCS1477 significantly inhibited tumor growth compared with vehicle. This occurred in a dose-dependent manner with the most effective tolerated dose being 20 mg/kg. CCS1477 reduced the transcription of key target genes *in vivo* including C-MYC and TMPRSS2 at 7 days; these changes were maintained at 28 days. Target protein expression (AR-FL, AR-V7, and C-MYC) was also downregulated at 7 days, and both AR-FL and AR-V7 were reduced at 28 days. RNA-sequencing analyses showed decreased AR-regulated gene expression. Interestingly, when we continued to measure tumor volume after stopping drug treatment, we observed an unusually long continuation of tumor inhibition, although the concentration of CCS1477 in plasma and tumor was undetectable 24 hours after the last dose and CCS1477 is not an irreversible inhibitor. This may support the use of intermittent dosing to maximize tolerability without compromising benefit and warrants clinical investigation. Antitumor activity was also observed in the CP50c PDX model; CCS1477 at 20 mg/kg

QD increased median time to 300% growth from 38 to 56 days; mRNA analyses confirmed (day 8) reduction in AR and C-MYC signaling. Finally, we acquired preliminary data from an ongoing first-in-human phase I trial (NCT03568656) in which men with mCRPC, heavily pretreated and resistant to standard therapies, were given oral CCS1477. Pharmacodynamic studies on pre- and postdose tumor biopsies demonstrated target engagement with drug-induced reductions in C-MYC protein; patient 1 also had decreased AR-V7 and C-MYC protein expression with a concomitant drop in serum KLK3, whereas patient 2 had decreased C-MYC and Ki-67, with a stable KLK3.

While we have targeted the bromodomain of these paralogs, we recognize that they can also be targeted at the conserved histone acetyltransferase (HAT) catalytic domains or the CH1/TAZ binding domains, which may have different biological consequences. For example, targeting the p300/CBP bromodomain reduces acetylation of H3K27 specifically at enhancers, whereas targeting the HAT catalytic domain has broader impact, reducing acetylation of H3K18 as well as H3K27 (53). We note that HAT inhibitors of p300/CBP, C646, and A-485 also induce cell death in androgen-dependent and CRPC cell lines (35, 54); these compounds do not, however, have drug-like properties supporting clinical development. We also recognize that p300/CBP siRNA knockdown was not completely replicated by CCS1477, and therefore inhibiting the bromodomain may uniquely block the function of these proteins.

The clinical development of p300/CBP inhibitors may face other challenges. First, CBP and p300 inhibition may have an on-target impact on platelets, albeit reversible, and may require intermittent dose scheduling, which is supported by the prolonged disease control seen after stopping CCS1477 in our 22Rv1 mouse xenograft model (55). Second, predictive biomarkers may be needed to identify which patients gain maximal clinical benefit from these agents; both SPOP mutations and C-MYC overexpression are reported to contribute to resistance to p300/CBP inhibition and need further investigation (56, 57). Finally, drug combinations may be necessary for their optimal clinical use; we report on CCS1477 administered with enzalutamide, whereas others have noted the potential for concomitant p300/CBP inhibition with anti–PD-1 therapy (58). Studies exploring mechanisms of acquired resistance are also needed, including studies of desensitization by p300/CBP overexpression or through redundant alternative transcriptional coactivators enabling activated AR to continue driving target gene expression.

In conclusion, targeting AR signaling through its coactivators p300 and CBP via their bromodomain offers a new therapeutic strategy that merits evaluation in advanced prostate cancer clinical trials in single agent and combination. Our early clinical findings that CCS1477 modulates plasma KLK3 levels and reduces expression of key therapeutic targets in advanced prostate cancer provide encouragement in the ongoing development of these agents.

METHODS

Patient Sample Collection

Patients were identified from a population of men with mCRPC treated at the Royal Marsden Hospital. All patients had given written informed consent and were enrolled in institutional protocols approved by the Royal Marsden (London, UK) ethics review committee (reference no. 04/Q0801/60). Human biological samples were sourced ethically and their research use was in accordance with the terms of the informed consent provided. We analyzed 43 patients with sufficient formalin-fixed, paraffin-embedded (FFPE) diagnostic (archival) castration-sensitive biopsies, and matched FFPE CRPC biopsies (Supplementary Table S3). All CSPC biopsies demonstrated adenocarcinoma and were from either prostate needle biopsy (n = 34), transurethral resection of the prostate (TURP; n = 3), or prostatectomy (n = 6). CRPC tissue was obtained from metastatic biopsies of bone (n = 26), lymph node (n = 15), soft tissue (n = 1), or TURP (n = 1). Additionally, pre- and postdose biopsies were collected for two patients with mCRPC enrolled in an ongoing first-in-human phase I trial of CCS1477 (NCT03568656). Patient 1 was on a schedule of 50 mg CCS1477 BD on a 3-day-on and 4-day-off schedule. The predose biopsy (lymph node) was collected in the second cycle on C2-D14 (at the end of 4 days off, allowing for complete washout of CCS1477) and the postdose biopsy sample (lymph node) was collected 4 hours after drug administration on C2-D15. Patient 2 was on a schedule of 25 mg CCS1477 BD continuously, and a biopsy (lymph node) was taken prior to trial initiation and then 3 hours after drug administration on C1-D15 (lymph node). Demographic and clinical data for each patient were retrospectively collected from the hospital's electronic patient record system.

IHC

All tissue blocks were freshly sectioned and considered for IHC analyses of CBP, p300, AR-FL, AR-V7, KLK3, Ki-67, or C-MYC only if adequate material was present (≥50 tumor cells; reviewed by pathologist B. Gurel). More specific details on the IHC assays used are available in Supplementary Table S9. Nuclear and/or cytoplasmic protein expression was determined for each case by a pathologist (B. Gurel) blinded to clinical data using the modified HS method, a semiquantitative assessment of staining intensity that reflects antigen concentration. HS was determined according to the formula: [(% of no staining) × 0] + [(% of weak staining) × 1] + [(% of moderate staining) × 2] + [(% of strong staining) × 3], yielding a range from 0 to 300 (59). Ki-67 was reported as a percentage of cells positive for protein expression.

Cell Lines

All cell lines used in this study were grown in recommended media at 37°C in 5% CO_2 and are detailed in Supplementary Table S10. All cell lines were tested for *Mycoplasma* using the VenorGem One Step PCR Kit (Cambio) and STR-profiled using the cell authentication service by Eurofins Medigenomix.

Development of JQ1-Resistant 22Rv1 Cell Line

22Rv1 cells were cultured in the presence of JQ1 or vehicle control (0.1% DMSO). JQ1 doses were escalated from 30 nmol/L (approximate IC_{90} concentration) to 500 nmol/L over the course of 6 months. JQ1 dose was escalated when cells had good morphology, viability, and growth rate and had been passaged at least twice in the preceding dose.

Development of Doxycycline-Inducible Cell Lines and CBP/p300 Reexpression

For generation of inducible (shCON, shCBP, and shp300) cell lines, 22Rv1 and C4-2 cells were transduced with SMARTvector Human Inducible nontargeting mCMV-TurboGFP control shRNA, CBP shRNA (Dharmacon V3SH11255-01EG1387), and p300 shRNA (Dharmacon V3SH11255-01EG2033) lentiviral vectors. Transduced cells underwent at least three rounds of antibiotic selection with

puromycin and were validated for respective knockdown with 10 ng doxycycline. Expression plasmids for CBP (OriGene Technologies, RC219036) and p300 (OriGene Technologies, RC223265) were used for protein reexpression experiments in doxycycline-inducible cell lines developed.

CCS1477

CCS1477 was synthesized according to processes described in the International Patent Application, publication number WO2018073586. For *in vitro* studies, CCS1477 was prepared as a 10 mmol/L stock solution in DMSO and diluted in relevant assay media to obtain a final assay concentration of <0.1% DMSO. For *in vivo* studies, CCS1477 was formulated in 5% DMSO:95% methylcellulose (0.5% w/v) and administered by oral gavage; 5% DMSO:95% methylcellulose (0.5% w/v) was used in *in vivo* studies as vehicle controls.

In Vitro *Binding Assays*

The affinity of CCS1477 binding to p300, CBP, or BRD4 bromodomains was calculated from an assessment of kinetic binding parameters in an SPR assay. CCS1477 binding was determined using a five-point log dilution from 10,000 to 1 nmol/L. In-cell target engagement of CCS1477 to the p300 and BRD4 bromodomains was determined using a proximity-based NanoBRET assay (Promega), which measured the ability of CCS1477 to inhibit the interaction between Histone H3.3 and p300 or BRD4 in transiently transfected HEK293 cells. CCS1477 inhibition of p300 or BRD4 binding to cellular histones was measured over a concentration range of 10,000 to 1 nmol/L.

In Vitro *Cell Line Proliferation Studies*

In vitro antiproliferative activity was measured in various prostate cancer cells treated with CCS1477 or BET inhibitors (JQ1, OTX-015, and I-BET151), specific siRNA or doxycycline-inducible shRNA (with or without CBP or p300 reexpression) using CyQuant (Thermo Fisher Scientific), CellTiter-Glo (Promega), or Quanti-IT Pico Green dsDNA assay kit (Thermo Fisher Scientific) according to the manufacturer's instructions.

In Vivo *Pharmacokinetic Analyses*

The *in vivo* pharmacokinetic properties of CCS1477 were determined in male CD1 mice after oral administration of 3 and 30 mg/kg. CCS1477 was formulated in 5% DMSO:95% methylcellulose (0.5% w/v in water) and dosing was administered by oral gavage. Blood samples were collected up to 12 hours following dosing for the measurement of blood concentrations of CCS1477 by LC-MS/MS.

In Vivo *Cell Line Mouse Xenograft Studies*

All animals were housed in pathogen-free facilities. All mouse work was approved by the Axis BioServices Animal Welfare and Ethical Review Committee and conducted under license and within the guidelines of the Home Office Animals (Scientific Procedures) Act 1986. Prostate xenograft tumors were established by subcutaneous injection of either 22Rv1 or LNCaP-Bic cells into noncastrated male athymic nude mice. Once tumors had reached approximately 150 mm^3, animals were randomized into control and treated groups. In all studies, tumor volume (measured by caliper), animal body weight, and condition were monitored at least twice weekly. Tumor samples were collected for analyses of pharmacodynamics biomarkers.

In Vivo *Patient-Derived Mouse Xenograft Studies*

All animals were housed in pathogen-free facilities. All mouse work was carried out in accordance with the Institute of Cancer Research (ICR) guidelines, including approval by the ICR Animal Welfare and Ethical Review Body, and with the UK Animals (Scientific Procedures) Act 1986. The CP50 PDX was derived from a metastatic lymph node biopsy from a patient with CRPC who had received all standard-of-care therapies for prostate cancer as previously described (44). A further subset of CP50 PDX was developed that was grown and maintained exclusively in castrate mice and given the designation CP50c PDX. For short-term analysis, CP50c PDX fragments were grafted subcutaneously into NOD/SCID gamma (NSG) male castrated mice, and drug treatment commenced by oral gavage when tumors reached a size of 300 to 400 mm^3. Mice were treated QD for 8 days, after which tumors were harvested for analyses (short term). For long-term analysis, CP50c PDX fragments from CP50c PDX tumors that had been passaged twice in castrated mice were grafted subcutaneously into castrated male NSG mice. Animals were treated with oral gavage when tumors reached a size of around 300 to 400 mm^3. Measurements were taken every 2–3 days (and grouped by 5-day intervals), and the experiment was terminated once tumors had reached a size of 1,200 mm^3.

Western Blotting (Cell Line, 22Rv1 Xenograft Model, and CP50c Mouse Xenograft Model)

Cells were lysed with RIPA buffer (Pierce) supplemented with protease inhibitor cocktail (Roche) and PhosStop phosphatase inhibitor mix (Roche). PDX lysate was obtained by mechanical homogenization, and reconstituted in RIPA buffer. Protein extracts (20 μg) were separated on 4%–12% NuPAGE Bis-Tris gel (Invitrogen) by electrophoresis and subsequently transferred onto Immobilon-P PVDF membranes of 0.45 μm pore size (Millipore). Details of primary antibodies used are provided in Supplementary Table S11. Chemiluminescence was detected on the Chemidoc Touch imaging system (Bio-Rad).

Western Blotting (Doxycycline-Inducible Cell Lines and CBP/p300 Reexpression)

Cell lysates were extracted as previously described (60). Lysate (40–50 μg) was resolved by SDS-PAGE, transferred to PVDF (polyvinylidene fluoride) membrane, and analyzed using CBP (Cell Signaling, D6C5), p300 (Active Motif, 61401), AR-FL and AR-V7 by molecular weight (Bethyl Laboratories, N20), C-MYC (Santa Cruz, 9E10), and GAPDH (Santa Cruz, 6C5) at 1:1,000 dilution.

RNA Extraction

Cell line RNA was extracted using the RNeasy Plus Mini Kit (Qiagen) as per the manufacturer's instructions. PDX RNA was obtained by mechanical homogenization, reconstituted with RNeasy RLT buffer, passed through a Qiashredder tube (Qiagen), and further processed with RNeasy Plus Mini Kit as above.

siRNA

Cells were transiently transfected with siRNA as indicated. All siRNA were ON-TARGETplus pools (Dharmacon; Horizon), listed in Supplementary Table S12. The siRNA was used along with 0.4% mRNAiMax transfection reagent (Thermo Fisher Scientific) as per the manufacturer's instructions and incubated with cells as indicated.

Quantitative Reverse Transcription PCR (Cell Line and CP50c Mouse Xenograft Models)

cDNA was synthesized using the Revertaid First-Strand cDNA Synthesis Kit (Thermo Fisher Scientific). Quantitative reverse transcription PCR (qRT-PCR) was carried out using a ViiA 7 Real-Time PCR System (Life Technologies) using the TaqMan Universal PCR Master Mix (Applied Biosystems). TaqMan probes (Thermo Fisher Scientific) used are listed in Supplementary Table S13. Fold change in mRNA expression levels was calculated by the comparative Ct

method, using the formula 2−(−(ΔΔCt). Cell line and CP50c mouse xenograft models were normalized against the average of the three housekeeping genes GAPDH, B2M, and HPRT1.

qRT-PCR (Doxycycline-Inducible Cell Lines and CBP/p300 Reexpression)

TRIzol (Invitrogen) was used to isolate RNA and SuperScript VILO (Invitrogen) was used to generate cDNA following manufacturer's instructions. PowerSybr (Thermo Fisher) and the ABI StepOne Real-Time PCR system were utilized in accordance with the manufacturer's specifications to perform quantitative PCR (qPCR) analyses. Primers used are listed in Supplementary Table S14.

ChIP

22Rv1 and C4-2 cells were plated in hormone-deficient media for 72 hours, following which cells were treated with vehicle (0 nmol/L) or CCS1477 500 nmol/L for 5 hours, followed by the addition of 10 nmol/L dihydrotestosterone for 3 hours. ChIP was performed as previously described (61). Briefly, cells were cross-linked with 1% fresh formaldehyde for 10 minutes at room temperature. Chromatin was sheared to 200–700 bp using Diagenode Ultrasonicator for 30 cycles. Lysates were incubated with CBP or p300 custom antibody, or AR-FL antibody (Millipore, 06-680). ChIP DNA was extracted via phenol-chloroform method and qPCR was performed using PowerUP SYBR (Thermo Fisher). Genes selected for ChIP-qPCR were prioritized on the basis of statistically significant transcriptional downregulation after CCS1477 treatment (1.5-fold change; $P \leq 0.05$) and known AR regulation: KLK3, TMPRSS2, FKBP5, ANKRD30B, CHRNA2 (with TFF1 and TGFA representing known CBP binding sites; refs. 48, 49). Primers were designed at AR target genes using previously described AR-binding sites and are listed in Supplementary Table S15 (62–64).

qRT-PCR (22Rv1 Xenograft Model)

A High-Capacity cDNA Reverse Transcription Kit (Thermo Fisher) was used to generate cDNA with preamplification of target sequences performed using TaqMan Preamp Master Mix (Thermo Fisher), both according to the manufacturers' instructions. PCR reactions were set up using TaqMan Master Mix (Thermo Fisher) and diluted pre-amplification reaction according to the manufacturers' instructions using TaqMan primer probe sets specific for the relevant target genes, listed in Supplementary Table S13. Analyses were performed using Bio-Rad CFX manager software, and all data were normalized relative to housekeeping genes GAPDH and RPLP0 before normalization to vehicle control.

Plasma KLK3

Total and free KLK3 was measured by ELISA in 50 μL serum (Abnova, KA0208 and KA0209), according to the manufacturer's instructions. Following incubation with appropriate antibodies and washing, absorbance was measured at 450 nm within 15 minutes of assay completion using a Varioskan LUC apparatus (Thermo Fisher). Controls were used to create a standard curve and total or free KLK3 quantified using ScanIT RE4.0 software.

RNA Sequencing and Analysis (22Rv1 Cell Line)

22Rv1 cells were seeded at equal density in hormone-deficient media. After 72 hours, cells were treated with either vehicle control, 100 nmol/L JQ1, or 96 nmol/L CCS1477. After 24 hours, cells were harvested and lysed, and RNA was extracted using TRIzol (Invitrogen), per the manufacturer's instructions. RNA-sequencing libraries were subsequently constructed using the TruSeq Stranded Total RNA Library Prep Gold Kit and sequenced on Illumina's NextSeq 500 sequencer at the Sidney Kimmel Cancer Sequencing core facility using single-end 75 bp reads. RNA-sequencing analysis was performed as previously described (65). Briefly, FASTQ files were aligned to the human genome (GRCh37/hg19) using STAR (version 2.5.2a), counts generated using featureCounts (version 1.5.0-p3), and differential expression, MA plots, and PCA performed using DESeq. RNA-sequencing data are accessible from The European Nucleotide Archive (www.ebi.ac.uk/ena) with accession number PRJEB41478.

RNA Sequencing and Analysis (22Rv1 Mouse Xenograft and CP50c PDX)

22Rv1 mouse xenograft and CP50c PDX RNA quality was analyzed using the Agilent Tapestation RNA ScreenTape. Total RNA (500 ng) from each sample was first used in the NEBNext rRNA Depletion Kit followed by the NEBNext Ultra II Directional RNA Library Prep Kit, according to the manufacturer's instructions. Library quality was confirmed using the Agilent Tapestation High Sensitivity DNA ScreenTape. The libraries were quantified and normalized by qPCR using the KAPA Library Quantification Kit (Roche). Library clustering was performed on a cBot with Illumina HiSeq PE Cluster Kit v3. The libraries were sequenced as paired-end 101 base pair reads on an Illumina HiSeq 2500 with an Illumina HiSeq SBS Kit v3. Base calling and quality scoring were performed using Real-Time Analyses (version 1.18.64) and FASTQ file generation and demultiplexing using CASAVA. 22Rv1 mouse xenograft and CP50c PDX reads were aligned to human GRCh37/hg19 and mouse mm9 genome using Tophat2 (v2.0.7). Gene expression, fragments per kilobase of transcript per million mapped reads (FPKM), was calculated using Cufflinks (66). Androgen response (Hallmark; H) was an accumulation measurement of AR pathway activity based on 100 genes regulated derived from the Hallmark Androgen Response gene set from the Molecular Signatures Database v7.1 (www.gsea-msigdb.org/; Supplementary Table S16; refs. 46, 47). AR signature was an accumulation measurement of AR pathway activity based on 43 genes regulated by AR in prostate cancer cell lines and metastatic prostate cancer patient samples as previously described (Supplementary Table S1; ref. 44). AR-V7 signature was an accumulation measurement of 59 genes that are associated with AR-V7 protein expression in CRPC biopsies as previously described (Supplementary Table S17; ref. 24). Signature scores were derived from the sum of *z*-score for the signature genes. RNA-seq data are accessible from The European Nucleotide Archive (www.ebi.ac.uk/ena) with accession number PRJEB41478.

Prostate Cancer Patient Transcriptome Analysis

Data from CRPC transcriptomes, generated by the International Stand Up To Cancer/Prostate Cancer Foundation (SU2C/PCF) Prostate Cancer Dream Team, were reanalyzed (41). The Cancer Genome Atlas (TCGA) program data were downloaded from http://gdac.broadinstitute.org/runs/stddata__2016_01_28/data/PRAD/20160128/. SU2C/PCF transcriptome reads were aligned to the human reference genome, and genome expression was determined as above. Androgen response (Hallmark; H), AR signature, and AR-V7 signature are described above (24, 44, 46, 47). The acquired ADT resistance signature was an accumulation measurement of 49 putative AR target genes that do not respond to androgen stimulation, and associate with biochemical relapse, as previously described (Supplementary Table S2; ref. 43). Signature scores were derived from the sum of *z*-score for the signature genes.

Statistical Analyses

Spearman correlation was used to determine the association between CBP and p300 mRNA levels and other characteristics such as AR signature, acquired ADT resistance signature, and AR expression levels. For the analysis of patient biopsies, nuclear CBP and p300 protein levels were reported as median values with IQRs. For paired, same patient, CSPC and CRPC expression studies, the Wilcoxon matched-pair signed rank test was used to compare differences in

protein expression levels. The correlation between nuclear CBP and p300 protein expression, and both CBP and p300 with AR-FL and AR-V7 protein expression, was determined using Spearman correlation. Time to CRPC was defined as the time from diagnosis (date of diagnostic biopsy unless clinical diagnosis was recorded as >1 month prior to biopsy) to documented progression (radiologic, KLK3 or change of treatment) on luteinizing hormone-releasing hormone (LHRH) agonist alone or with antiandrogen if started before/or with LHRH agonist. Overall survival was defined as time from diagnosis (defined above) to date of death or last follow-up/contact. Patient outcomes were compared by nuclear CBP and p300 protein expression (H-score) at diagnosis; median overall survival and median time to CRPC were estimated using the Kaplan–Meier method, and respective hazard ratios were obtained by Cox regression. Unpaired Student *t* tests were used to determine differences between mRNA expression of control and treatment groups (CCS1477 or target siRNA) in cell line models. Unpaired Student *t* tests were used to determine differences between mRNA expression and relative growth of shCBP:EV compared with shCBP:CBP rescue, and shp300:EV compared with shp300:p300 rescue, in doxycycline-inducible shRNA cell line models. Unpaired Student *t* tests were used to determine differences between ChIP-qPCR studies of vehicle and CCS1477 treatment in cell line models. Unpaired Student *t* tests were used to determine differences in growth between mouse xenograft models treated with vehicle and various doses of CCS1477 at the time points indicated. No adjustment for multiple testing has been made. Analysis and presentation of all data were made using GraphPad Prism v7, and all statistical analyses are detailed in individual figure legends.

Authors' Disclosures

A. Sharp reports other support from Roche-Genentech and Astellas outside the submitted work. N. Brooks reports grants from Innovate UK during the conduct of the study. W. West reports grants from Innovate UK during the conduct of the study. B. Young reports other support from CellCentric Ltd during the conduct of the study. M. Raja reports other support from CellCentric Ltd during the conduct of the study. J. Lane reports other support from CellCentric Ltd during the conduct of the study. S. Thomson reports other support from Cell Centric Ltd during the conduct of the study. J. Worthington reports other from Cellcentric during the conduct of the study. S. Onions reports other support from CellCentric Limited during the conduct of the study; in addition, S. Onions has a patent 10696666 issued. J. Shannon reports other support from CellCentric Ltd during the conduct of the study; in addition, J. Shannon has a patent 10696666 issued. S. Paoletta reports other support from CellCentric Ltd during the conduct of the study; personal fees from Sygnature Discovery Ltd and personal fees from Evotec SE outside the submitted work; in addition, S. Paoletta has a patent 10696666 issued. R. Brown reports other support from CellCentric Ltd during the conduct of the study; in addition, R. Brown has a patent for 10696666 issued. D. Smyth reports other support from Cellcentric Ltd during the conduct of the study; in addition, D. Smyth has a patent for patent 10696666 issued. G.W. Harbottle reports other support from Sygnature Discovery Ltd during the conduct of the study; in addition, G.W. Harbottle has a patent 10696666 issued. D. Taddei reports other from CellCentric Ltd during the conduct of the study; in addition, D. Taddei has a patent 10696666 issued. K.E. Knudsen reports grants from CellCentric during the conduct of the study; and K.E. Knudsen reports the following unrelated disclosures for the period over the last 3 years: research support from Celgene, Novartis and consultant/advisory relationships with Sanofi, Celgene, Janssen, and Genentech. N. Pegg reports grants from Innovate UK during the conduct of the study; in addition, N. Pegg has a patent 10696666 issued. J.S. de Bono reports grants from CellCentric during the conduct of the study; grants and personal fees from Daiichi Sankyo, AstraZeneca, Pfizer, Bayer Oncology, MSD, Merck Serono, Harpoon, and Genentech/Roche, personal fees from Eisai and Constellation, and grants from Sun Pharma outside the submitted work; in addition, J.S. de Bono has a patent for Abiraterone licensed and with royalties paid from Janssen. No other disclosures were reported.

Authors' Contributions

J. Welti: Conceptualization, data curation, formal analysis, validation, investigation, visualization, methodology, writing–original draft, writing–review and editing. **B. Gurel:** Data curation, validation, investigation, visualization, methodology, writing–review and editing. **J. Rekowski:** Data curation, validation, investigation, visualization, methodology, writing–review and editing. **D. Bogdan:** Data curation, software, validation, investigation, methodology, writing–review and editing. **W. West:** Resources, funding acquisition, writing–review and editing. **B. Young:** Data curation, investigation, and methodology. **M. Raja:** Investigation and methodology. **A. Prosser:** Investigation. **J. Lane:** Investigation. **S. Thomson:** Supervision, validation, and investigation. **J. Worthington:** Supervision, investigation, and methodology. **A. Sharp:** Conceptualization, data curation, formal analysis, funding acquisition, validation, investigation, visualization, methodology, writing–original draft, project administration, writing–review and editing. **S. Onions:** Supervision, investigation, and methodology. **J. Shannon:** Investigation and methodology. **S. Paoletta:** Investigation and methodology. **R. Brown:** Investigation and methodology. **D. Smyth:** Investigation and methodology. **G.W. Harbottle:** Investigation and methodology. **V.S. Gil:** Methodology, writing–review and editing. **S. Miranda:** Writing–review and editing. **M. Crespo:** Writing–review and editing. **A. Ferreira:** Writing–review and editing. **N. Brooks:** Conceptualization, supervision, writing–original draft, and project administration. **R. Pereira:** Writing–review and editing. **N. Tunariu:** Writing–review and editing. **S. Carreira:** Formal analysis, methodology, writing–review and editing. **A.J. Neeb:** Methodology, writing–review and editing. **J. Ning:** Methodology, writing–review and editing. **A. Swain:** Methodology, writing–review and editing. **D. Taddei:** Data curation, investigation, and methodology. **S. International Dream Team:** Resources. **M.J. Schiewer:** Data curation, formal analysis, validation, methodology, writing–review and editing. **K.E. Knudsen:** Conceptualization, resources, supervision, writing–original draft, writing–review and editing. **W. Yuan:** Data curation, software, formal analysis, validation, investigation, visualization, methodology, writing–review and editing. **N. Pegg:** Conceptualization, supervision, writing–original draft, writing–review and editing. **J.S. de Bono:** Conceptualization, resources, supervision, funding acquisition, writing–original draft, project administration, writing–review and editing. **C. McNair:** Data curation, software, formal analysis, validation, investigation, visualization, methodology, writing–review and editing. **S.N. Chand:** Data curation, formal analysis, validation, investigation, visualization, methodology, writing–review and editing. **A. Pal:** Data curation, validation, investigation, methodology, writing–review and editing. **I. Figueiredo:** Data curation, validation, investigation, visualization, methodology, writing–review and editing. **R. Riisnaes:** Data curation, validation, investigation, visualization, and methodology.

Acknowledgments

Work in the JdB laboratory was supported by funding from the Movember Foundation/Prostate Cancer UK (CEO13-2-002), the US Department of Defense, the Prostate Cancer Foundation (20131017 and 20131017-1), a Stand Up To Cancer–Prostate Cancer Dream Team Translational Research Grant (SU2C-AACR-DT0712), Cancer Research UK (CRM108X-A25144), the UK Department of Health through an Experimental Cancer Medicine Centre grant (ECMC-CRM064X), and research support from CellCentric Ltd. Stand Up To Cancer is a division of the Entertainment Industry Foundation. The indicated SU2C research grant is administered by the American

Association for Cancer Research, the scientific partner of SU2C. A. Sharp has been supported by the Medical Research Council, the Academy of Medical Sciences, Prostate Cancer UK, and is currently supported by the Prostate Cancer Foundation and Wellcome Trust. Work in the K.E. Knudsen's laboratory was supported by funding from the NCI (CA176401), the Prostate Cancer Foundation, and research support from CellCentric Ltd.

Received May 27, 2020; revised October 16, 2020; accepted December 11, 2020; published first January 11, 2021.

REFERENCES

1. Culp MB, Soerjomataram I, Efstathiou JA, Bray F, Jemal A. Recent global patterns in prostate cancer incidence and mortality rates. Eur Urol 2020;77:38–52.
2. Visakorpi T, Hyytinen E, Koivisto P, Tanner M, Keinanen R, Palmberg C, et al. In vivo amplification of the androgen receptor gene and progression of human prostate cancer. Nat Genet 1995;9:401–6.
3. Chen CD, Welsbie DS, Tran C, Baek SH, Chen R, Vessella R, et al. Molecular determinants of resistance to antiandrogen therapy. Nat Med 2004;10:33–9.
4. Abida W, Cyrta J, Heller G, Prandi D, Armenia J, Coleman I, et al. Genomic correlates of clinical outcome in advanced prostate cancer. Proc Natl Acad Sci U S A 2019;116:11428–36.
5. Beer TM, Armstrong AJ, Rathkopf DE, Loriot Y, Sternberg CN, Higano CS, et al. Enzalutamide in metastatic prostate cancer before chemotherapy. N Engl J Med 2014;371:424–33.
6. Ryan CJ, Smith MR, de Bono JS, Molina A, Logothetis CJ, de Souza P, et al. Abiraterone in metastatic prostate cancer without previous chemotherapy. N Engl J Med 2013;368:138–48.
7. de Bono JS, Logothetis CJ, Molina A, Fizazi K, North S, Chu L, et al. Abiraterone and increased survival in metastatic prostate cancer. N Engl J Med 2011;364:1995–2005.
8. James ND, de Bono JS, Spears MR, Clarke NW, Mason MD, Dearnaley DP, et al. Abiraterone for prostate cancer not previously treated with hormone therapy. N Engl J Med 2017;377:338–51.
9. Antonarakis ES, Lu C, Wang H, Luber B, Nakazawa M, Roeser JC, et al. AR-V7 and resistance to enzalutamide and abiraterone in prostate cancer. N Engl J Med 2014;371:1028–38.
10. De Laere B, van Dam PJ, Whitington T, Mayrhofer M, Diaz EH, Van den Eynden G, et al. Comprehensive profiling of the androgen receptor in liquid biopsies from castration-resistant prostate cancer reveals novel intra-AR structural variation and splice variant expression patterns. Eur Urol 2017;72:192–200.
11. Guedes LB, Morais CL, Almutairi F, Haffner MC, Zheng Q, Isaacs JT, et al. Analytic validation of RNA in situ hybridization (RISH) for AR and AR-V7 expression in human prostate cancer. Clin Cancer Res 2016;22:4651–63.
12. Guo Z, Yang X, Sun F, Jiang R, Linn DE, Chen H, et al. A novel androgen receptor splice variant is up-regulated during prostate cancer progression and promotes androgen depletion-resistant growth. Cancer Res 2009;69:2305–13.
13. Hu R, Lu C, Mostaghel EA, Yegnasubramanian S, Gurel M, Tannahill C, et al. Distinct transcriptional programs mediated by the ligand-dependent full-length androgen receptor and its splice variants in castration-resistant prostate cancer. Cancer Res 2012;72:3457–62.
14. Li Y, Chan SC, Brand LJ, Hwang TH, Silverstein KA, Dehm SM. Androgen receptor splice variants mediate enzalutamide resistance in castration-resistant prostate cancer cell lines. Cancer Res 2013;73:483–9.
15. Nakazawa M, Lu C, Chen Y, Paller CJ, Carducci MA, Eisenberger MA, et al. Serial blood-based analysis of AR-V7 in men with advanced prostate cancer. Ann Oncol 2015;26:1859–65.
16. Qu F, Xie W, Nakabayashi M, Zhang H, Jeong SH, Wang X, et al. Association of AR-V7 and prostate-specific antigen RNA levels in blood with efficacy of abiraterone acetate and enzalutamide treatment in men with prostate cancer. Clin Cancer Res 2017;23:726–34.
17. Scher HI, Graf RP, Schreiber NA, McLaughlin B, Lu D, Louw J, et al. Nuclear-specific AR-V7 protein localization is necessary to guide treatment selection in metastatic castration-resistant prostate cancer. Eur Urol 2017;71:874–82.
18. Scher HI, Lu D, Schreiber NA, Louw J, Graf RP, Vargas HA, et al. Association of AR-V7 on circulating tumor cells as a treatment-specific biomarker with outcomes and survival in castration-resistant prostate cancer. JAMA Oncol 2016;2:1441–9.
19. Todenhofer T, Azad A, Stewart C, Gao J, Eigl BJ, Gleave ME, et al. AR-V7 transcripts in whole blood RNA of patients with metastatic castration resistant prostate cancer correlate with response to abiraterone acetate. J Urol 2017;197:135–42.
20. Welti J, Rodrigues DN, Sharp A, Sun S, Lorente D, Riisnaes R, et al. Analytical validation and clinical qualification of a new immunohistochemical assay for androgen receptor splice variant-7 protein expression in metastatic castration-resistant prostate cancer. Eur Urol 2016;70:599–608.
21. Zhu Y, Sharp A, Anderson CM, Silberstein JL, Taylor M, Lu C, et al. Novel junction-specific and quantifiable in situ detection of AR-V7 and its clinical correlates in metastatic castration-resistant prostate cancer. Eur Urol 2018;73:727–35.
22. Hu R, Dunn TA, Wei S, Isharwal S, Veltri RW, Humphreys E, et al. Ligand-independent androgen receptor variants derived from splicing of cryptic exons signify hormone-refractory prostate cancer. Cancer Res 2009;69:16–22.
23. Sharp A, Porta N, Lambros MBK, Welti JC, Paschalis A, Raj GV, et al. Dissecting prognostic from predictive utility: circulating AR-V7 biomarker testing for advanced prostate cancer. J Clin Oncol 2019;37:2182–4.
24. Sharp A, Coleman I, Yuan W, Sprenger C, Dolling D, Rodrigues DN, et al. Androgen receptor splice variant-7 expression emerges with castration resistance in prostate cancer. J Clin Invest 2019;129:192–208.
25. Debes JD, Sebo TJ, Lohse CM, Murphy LM, Haugen DA, Tindall DJ. p300 in prostate cancer proliferation and progression. Cancer Res 2003;63:7638–40.
26. Comuzzi B, Nemes C, Schmidt S, Jasarevic Z, Lodde M, Pycha A, et al. The androgen receptor co-activator CBP is up-regulated following androgen withdrawal and is highly expressed in advanced prostate cancer. J Pathol 2004;204:159–66.
27. Chan HM, La Thangue NB. p300/CBP proteins: HATs for transcriptional bridges and scaffolds. J Cell Sci 2001;114:2363–73.
28. Fronsdal K, Engedal N, Slagsvold T, Saatcioglu F. CREB binding protein is a coactivator for the androgen receptor and mediates cross-talk with AP-1. J Biol Chem 1998;273:31853–9.
29. Aarnisalo P, Palvimo JJ, Janne OA. CREB-binding protein in androgen receptor-mediated signaling. Proc Natl Acad Sci U S A 1998;95:2122–7.
30. Fu M, Wang C, Reutens AT, Wang J, Angeletti RH, Siconolfi-Baez L, et al. p300 and p300/cAMP-response element-binding protein-associated factor acetylate the androgen receptor at sites governing hormone-dependent transactivation. J Biol Chem 2000;275:20853–60.
31. Reutens AT, Fu M, Wang C, Albanese C, McPhaul MJ, Sun Z, et al. Cyclin D1 binds the androgen receptor and regulates hormone-dependent signaling in a p300/CBP-associated factor (P/CAF)-dependent manner. Mol Endocrinol 2001;15:797–811.
32. Heemers HV, Debes JD, Tindall DJ. The role of the transcriptional coactivator p300 in prostate cancer progression. Adv Exp Med Biol 2008;617:535–40.
33. Ianculescu I, Wu DY, Siegmund KD, Stallcup MR. Selective roles for cAMP response element-binding protein binding protein and p300 protein as coregulators for androgen-regulated gene expression in advanced prostate cancer cells. J Biol Chem 2012;287:4000–13.
34. Jin L, Garcia J, Chan E, de la Cruz C, Segal E, Merchant M, et al. Therapeutic targeting of the CBP/p300 bromodomain blocks the growth of castration-resistant prostate cancer. Cancer Res 2017;77:5564–75.
35. Santer FR, Hoschele PP, Oh SJ, Erb HH, Bouchal J, Cavarretta IT, et al. Inhibition of the acetyltransferases p300 and CBP reveals a targetable function for p300 in the survival and invasion pathways of prostate cancer cell lines. Mol Cancer Ther 2011;10:1644–55.

36. Gruber M, Ferrone L, Puhr M, Santer FR, Furlan T, Eder IE, et al. p300 is up-regulated by docetaxel and is a target in chemoresistant prostate cancer. Endocr Relat Cancer 2020;27:187–98.
37. Isharwal S, Miller MC, Marlow C, Makarov DV, Partin AW, Veltri RW. p300 (histone acetyltransferase) biomarker predicts prostate cancer biochemical recurrence and correlates with changes in epithelia nuclear size and shape. Prostate 2008;68:1097–104.
38. Fu M, Rao M, Wang C, Sakamaki T, Wang J, Di Vizio D, et al. Acetylation of androgen receptor enhances coactivator binding and promotes prostate cancer cell growth. Mol Cell Biol 2003;23:8563–75.
39. Wang G, Jones SJ, Marra MA, Sadar MD. Identification of genes targeted by the androgen and PKA signaling pathways in prostate cancer cells. Oncogene 2006;25:7311–23.
40. Kumar A, Coleman I, Morrissey C, Zhang X, True LD, Gulati R, et al. Substantial interindividual and limited intraindividual genomic diversity among tumors from men with metastatic prostate cancer. Nat Med 2016;22:369–78.
41. Robinson D, Van Allen EM, Wu YM, Schultz N, Lonigro RJ, Mosquera JM, et al. Integrative clinical genomics of advanced prostate cancer. Cell 2015;161:1215–28.
42. Cancer Genome Atlas Research Network. The molecular taxonomy of primary prostate cancer. Cell 2015;163:1011–25.
43. Stelloo S, Nevedomskaya E, van der Poel HG, de Jong J, van Leenders GJ, Jenster G, et al. Androgen receptor profiling predicts prostate cancer outcome. EMBO Mol Med 2015;7:1450–64.
44. Welti J, Sharp A, Yuan W, Dolling D, Nava Rodrigues D, Figueiredo I, et al. Targeting bromodomain and extra-terminal (BET) family proteins in castration-resistant prostate cancer (CRPC). Clin Cancer Res 2018;24:3149–62.
45. Conery AR, Centore RC, Neiss A, Keller PJ, Joshi S, Spillane KL, et al. Bromodomain inhibition of the transcriptional coactivators CBP/EP300 as a therapeutic strategy to target the IRF4 network in multiple myeloma. Elife 2016;5:e10483.
46. Subramanian A, Tamayo P, Mootha VK, Mukherjee S, Ebert BL, Gillette MA, et al. Gene set enrichment analysis: a knowledge-based approach for interpreting genome-wide expression profiles. Proc Natl Acad Sci U S A 2005;102:15545–50.
47. Mootha VK, Lindgren CM, Eriksson KF, Subramanian A, Sihag S, Lehar J, et al. PGC-1alpha-responsive genes involved in oxidative phosphorylation are coordinately downregulated in human diabetes. Nat Genet 2003;34:267–73.
48. Ceschin DG, Walia M, Wenk SS, Duboe C, Gaudon C, Xiao Y, et al. Methylation specifies distinct estrogen-induced binding site repertoires of CBP to chromatin. Genes Dev 2011;25:1132–46.
49. Murakami S, Nagari A, Kraus WL. Dynamic assembly and activation of estrogen receptor alpha enhancers through coregulator switching. Genes Dev 2017;31:1535–48.
50. Asangani IA, Dommeti VL, Wang X, Malik R, Cieslik M, Yang R, et al. Therapeutic targeting of BET bromodomain proteins in castration-resistant prostate cancer. Nature 2014;510:278–82.
51. Asangani IA, Wilder-Romans K, Dommeti VL, Krishnamurthy PM, Apel IJ, Escara-Wilke J, et al. BET bromodomain inhibitors enhance efficacy and disrupt resistance to AR antagonists in the treatment of prostate cancer. Mol Cancer Res 2016;14:324–31.
52. Meyer SN, Scuoppo C, Vlasevska S, Bal E, Holmes AB, Holloman M, et al. Unique and shared epigenetic programs of the CREBBP and EP300 acetyltransferases in germinal center B cells reveal targetable dependencies in lymphoma. Immunity 2019;51:535–47.
53. Raisner R, Kharbanda S, Jin L, Jeng E, Chan E, Merchant M, et al. Enhancer activity requires CBP/P300 bromodomain-dependent histone H3K27 acetylation. Cell Rep 2018;24:1722–9.
54. Lasko LM, Jakob CG, Edalji RP, Qiu W, Montgomery D, Digiammarino EL, et al. Discovery of a selective catalytic p300/CBP inhibitor that targets lineage-specific tumours. Nature 2017;550:128–32.
55. Katavolos P, Cain G, Farman C, Romero FA, Magnuson S, Ly JQ, et al. Preclinical safety assessment of a highly selective and potent dual small-molecule inhibitor of CBP/P300 in rats and dogs. Toxicol Pathol 2020;48:465–80.
56. Coleman DJ, Gao L, Schwartzman J, Korkola JE, Sampson D, Derrick DS, et al. Maintenance of MYC expression promotes de novo resistance to BET bromodomain inhibition in castration-resistant prostate cancer. Sci Rep 2019;9:3823.
57. Yan Y, Ma J, Wang D, Lin D, Pang X, Wang S, et al. The novel BET-CBP/p300 dual inhibitor NEO2734 is active in SPOP mutant and wild-type prostate cancer. EMBO Mol Med 2019;11:e10659.
58. Liu J, He D, Cheng L, Huang C, Zhang Y, Rao X, et al. p300/CBP inhibition enhances the efficacy of programmed death-ligand 1 blockade treatment in prostate cancer. Oncogene 2020;39:3939–51.
59. Detre S, Saclani Jotti G, Dowsett M. A "quickscore" method for immunohistochemical semiquantitation: validation for oestrogen receptor in breast carcinomas. J Clin Pathol 1995;48:876–8.
60. Goodwin JF, Schiewer MJ, Dean JL, Schrecengost RS, de Leeuw R, Han S, et al. A hormone-DNA repair circuit governs the response to genotoxic insult. Cancer Discov 2013;3:1254–71.
61. McNair C, Urbanucci A, Comstock CE, Augello MA, Goodwin JF, Launchbury R, et al. Cell cycle-coupled expansion of AR activity promotes cancer progression. Oncogene 2017;36:1655–68.
62. Decker KF, Zheng D, He Y, Bowman T, Edwards JR, Jia L. Persistent androgen receptor-mediated transcription in castration-resistant prostate cancer under androgen-deprived conditions. Nucleic Acids Res 2012;40:10765–79.
63. Cai L, Tsai YH, Wang P, Wang J, Li D, Fan H, et al. ZFX mediates non-canonical oncogenic functions of the androgen receptor splice variant 7 in castrate-resistant prostate cancer. Mol Cell 2018;72:341–54.
64. Kron KJ, Murison A, Zhou S, Huang V, Yamaguchi TN, Shiah YJ, et al. TMPRSS2-ERG fusion co-opts master transcription factors and activates NOTCH signaling in primary prostate cancer. Nat Genet 2017;49:1336–45.
65. Dylgjeri E, McNair C, Goodwin JF, Raymon HK, McCue PA, Shafi AA, et al. Pleiotropic impact of DNA-PK in cancer and implications for therapeutic strategies. Clin Cancer Res 2019;25:5623–37.
66. Trapnell C, Roberts A, Goff L, Pertea G, Kim D, Kelley DR, et al. Differential gene and transcript expression analysis of RNA-seq experiments with TopHat and Cufflinks. Nat Protoc 2012;7:562–78.